Food Research International 170 (2023) 112963

Contents lists available at ScienceDirect

Food Research International

journal homepage: www.elsevier.com/locate/foodres

Metabolomic insights into phenolics-rich chestnut shells extract as a nutraceutical ingredient – A comprehensive evaluation of its impacts on oxidative stress biomarkers by an *in-vivo* study

Diana Pinto [a], Anallely López-Yerena [b,c], Andreia Almeida [a], Bruno Sarmento [d,e,f], Rosa Lamuela-Raventós [b,g], Anna Vallverdú-Queralt [b,c,g,*], Cristina Delerue-Matos [a], Francisca Rodrigues [a,*]

[a] *REQUIMTE/LAQV, ISEP, Polytechnic of Porto, Rua Dr. António Bernardino de Almeida, 4249-015 Porto, Portugal*
[b] *Polyphenol Research Group, Department of Nutrition, Food Science and Gastronomy XIA, Faculty of Pharmacy and Food Sciences, University of Barcelona, 08028 Barcelona, Spain*
[c] *Institute of Nutrition and Food Safety (INSA-UB), University of Barcelona, Barcelona, Spain*
[d] *i3S – Institute for Research and Innovation in Health, University of Porto, Rua Alfredo Allen, 208, 4200-135 Porto, Portugal*
[e] *INEB – Institute of Biomedical Engineering, University of Porto, Rua Alfredo Allen, 208, 4200-135 Porto, Portugal*
[f] *CESPU – Institute for Research and Advanced Training in Health Sciences and Technologies, Rua Central de Gandra 1317, 4585-116 Gandra, Portugal*
[g] *Consorcio CIBER, M.P. Fisiopatología de la Obesidad y la Nutrición (CIBERObn), Instituto de Salud Carlos III (ISCIII), Madrid, Spain*

A R T I C L E I N F O

Keywords:
Castanea sativa
Antioxidants
Anti-aging compounds
Oxidative stress-mediated pathologies
Metabolomic fingerprinting

A B S T R A C T

The present study attempted for the first time to explore the effects of the daily oral intake of a phenolics-rich extract from chestnut shells (CS) on the metabolomic profiling of rat tissues by liquid chromatography coupled to Orbitrap-mass spectrometry (LC-ESI-LTQ-Orbitrap-MS) targeted to polyphenolics and their metabolites and screen potential oxidative stress biomarkers, validating its use as a promising nutraceutical ingredient with outstanding antioxidant properties for the prevention and co-therapy of lifestyle-related diseases triggered by oxidative stress. The results demonstrated new insights into the metabolomic fingerprinting of polyphenols from CS, confirming their absorption and biotransformation by phase I (hydrogenation) and II (glucuronidation, methylation, and sulfation) enzymes. Phenolic acids were the main polyphenolic class, followed by hydrolyzable tannins, flavanols, and lignans. In contrast to the liver, sulfated conjugates were the principal metabolites reaching the kidneys. The multivariate data analysis predicted an exceptional contribution of polyphenols and their microbial and phase II metabolites to the *in-vivo* antioxidant response of the CS extract in rats, recommending its use as an appealing source of anti-aging molecules for nutraceuticals. This is the first study that explored the relation between metabolomic profiling of rat tissues and *in-vivo* antioxidant effects after oral treatment with a phenolics-rich CS extract.

Abbreviations: ACN, acetonitrile; b.w., body weight; CA, caffeic acid; CAT, Catalase; ChlorogenAc, chlorogenic acid; CinnamAc, cinnamic acid; *m*-CoumAc, *m*-coumaric acid; *o*-CoumAc, *o*-coumaric acid; *ρ*-CoumAc, *ρ*-coumaric acid; CS, chestnut shells; DHBA, dihydroxybenzoic acid; DHCA, dihydrocaffeic acid; DHFA, dihydroferulic acid; DHPPA, dihydroxyphenylpropionic acid; EntD, enterodiol; EntL, enterolactone; FA, ferulic acid; GA, gallic acid; GSH, reduced glutathione; GSH-Px, glutathione peroxidase; HBA, hydroxybenzoic acid; HBAs, hydroxybenzoic acids; HCAs, hydroxycinnamic acids; HippurAc, hippuric acid; HPAA, hydroxyphenylacetic acid; HPAAs, hydroxyphenylacetic acids; HPPA, hydroxyphenylpropionic acid; HPPAs, hydroxyphenylpropanoic acids; LC-ESI-LTQ-Orbitrap-MS, liquid chromatography coupled to Orbitrap-mass spectrometry LPO, lipid peroxidation; MCP-1, monocyte chemoattractant protein-1; NF-κB, nuclear factor κB; PAA, phenylacetic acid; PAI-1, plasminogen activator inhibitor type-1; PC, Principal component; PCA, Principal component analysis; PVA, phenylvaleric acids; PVL, phenylvalerolactones; SinapAc, sinapic acid; SOD, superoxide dismutase; SWE, Subcritical Water Extraction; SyrAc, syringic acid; UDP, uridine diphosphate; Uro, urolithin; TNF-α, tumor necrosis factor-α.

* Corresponding authors at: Nutrition, Food Science and Gastronomy Department, School of Pharmacy and Food Science, University of Barcelona, Av Joan XXIII s/n 08028 Barcelona, Barcelona, Spain (A. Vallverdú-Queralt). REQUIMTE/LAQV, ISEP, Polytechnic of Porto, Rua Dr. António Bernardino de Almeida, 431, 4249-015 Porto, Portugal (F. Rodrigues).

E-mail addresses: avallverdu@ub.edu (A. Vallverdú-Queralt), francisca.rodrigues@graq.isep.ipp.pt (F. Rodrigues).

https://doi.org/10.1016/j.foodres.2023.112963
Received 11 February 2023; Received in revised form 17 April 2023; Accepted 10 May 2023
Available online 15 May 2023

1. Introduction

Inflammation and oxidative stress are potentially major risk factors for the development of chronic diseases, including cancer, neurodegenerative, cardiovascular, and metabolic pathologies (Charles et al., 2021). Oxidative stress results from the imbalance between the overproduction of pro-oxidant reactive species and the antioxidant defense capacity of cells, namely enzymatic (i.e., catalase (CAT), glutathione peroxidase (GSH-Px) and superoxide dismutase (SOD)) and non-enzymatic antioxidants (i.e., reduced glutathione (GSH)), favoring the accumulation of reactive species with deleterious effects in biological tissues (Pinto, Cádiz-Gurrea, Vallverdú-Queralt, et al., 2021).

A high dietary intake of fruits and vegetables enriched in antioxidants (such as polyphenols) has unveiled a close relationship with preventive effects against oxidative stress-mediated diseases (Martins et al., 2016; Pinto, Cádiz-Gurrea, Vallverdú-Queralt, et al., 2021). Polyphenols are plant secondary metabolites with pronounced bioactivity documented in animals and humans (Charles et al., 2021; Martins et al., 2016). The metabolic effects of polyphenols have been extensively evaluated by *in-vivo* studies through measuring the concentrations of glucose, lipids, and other oxidative stress biomarkers in blood (Martins et al., 2016; Noh et al., 2010, 2011; Pinto et al., 2023). Even so, these biomarkers may provide inconsistent findings and fail to reflect the full diversity of metabolic effects (Martins et al., 2016). Nevertheless, polyphenols are poorly absorbed, owing to limited bioavailability and extensive metabolism across different organs (A. López-Yerena et al., 2021; Martins et al., 2016). For instance, lower bioactivity has been suggested for polyphenols that undergo phase II metabolism, whereas the biotransformation into aglycones allows better intestinal absorption via gut microbiota (A. López-Yerena et al., 2021; Marhuenda-Muñoz et al., 2019). The interaction polyphenols–gut microbiota may also deliver positive effects against several diseases (Corrêa et al., 2019; Martins et al., 2016). Hence, the hypothesis that polyphenols exhibit a direct scavenging activity on radicals is constrained. Beyond the well-documented anti-radical properties, numerous mechanisms have evidenced the efficacy of polyphenols in modulating antioxidant and detoxifying enzymes activities, encompassing the first defense system under oxidative stress conditions (Martins et al., 2016; Pinto, Cádiz-Gurrea, Vallverdú-Queralt, et al., 2021).

Chestnut (*Castanea sativa*) shells (CS) are an appealing source of bioactive compounds (i.e., polyphenols and vitamin E), embracing promissory antioxidant properties (Pinto, Cádiz-Gurrea, Vallverdú-Queralt, et al., 2021). This underexploited agro-industrial residue is generated in huge amounts during chestnut fruit processing. Most studies on CS have only explored their phytochemical composition and *in-vitro* bioactivity (Lameirão et al., 2020; Pinto, Cádiz-Gurrea, Garcia, et al., 2021; Pinto & Cádiz-Gurrea et al., 2020; Pinto, Silva, et al., 2021; Pinto, Vieira, et al., 2021). Despite the *in-vivo* bioactivity of other chestnut species has been extensively investigated (Noh et al., 2010, 2011), only one study was conducted on CS, attesting antioxidant effects on rat tissues by upmodulating antioxidant enzymes' activities and downregulating lipid peroxidation (LPO) without histopathological alterations (Pinto et al., 2023). The bioactivity of CS was mainly attributed to the phenolic composition with attractive applications in nutraceuticals (Pinto & Cádiz-Gurrea et al., 2020; Pinto, Cádiz-Gurrea, Vallverdú-Queralt, et al., 2021; Pinto, Vieira, et al., 2021). Given the broad scope of pharmacological effects, CS revealed anti-inflammatory, antimicrobial, antioxidant, hypolipidemic, hypoglycemic, and neuroprotective properties (Pinto, Cádiz-Gurrea, Garcia, et al., 2021; Pinto, Silva, et al., 2021).

Metabolomics has arisen as a hot research topic in the pharmaceutical and nutraceutical fields to comprehend the causal role of bioactive molecules in preventing lifestyle-related diseases and attenuating premature aging effects (Charles et al., 2021). Hence, the metabolites may be recognized as potential oxidative stress biomarkers (Charles et al., 2021). Although metabolomic studies in biological tissues are still scarce, this approach comprises a valuable tool for a deep insight into the biotransformation of polyphenols, underlying their *in-vivo* bioactivity.

The purpose of this study was to explore the effects of the daily oral intake of phenolics-rich CS extract on the metabolomic profiling of rat tissues by liquid chromatography coupled to Orbitrap-mass spectrometry (LC-ESI-LTQ-Orbitrap-MS), valorizing it as a prominent nutraceutical ingredient for the prevention and co-therapy of oxidative stress-mediated pathologies. The relationship between phenolic metabolites and potential oxidative stress biomarkers, namely LPO, SOD, CAT, and GSH-Px activities, was ascertained through multivariate data analysis. This is the first study that offers an in-depth assessment of the metabolomic fingerprinting of different tissues from rats orally treated with a nutraceutical extract from CS.

2. Materials and methods

2.1. Chemicals

Standards were supplied as follows: caffeic acid (CA), catechol, chlorogenic acid (ChlorogenAc), cinnamic acid (CinnamAc), *o*-coumaric acid (*o*-CoumAc), *m*-coumaric acid (*m*-CoumAc), 2,5-dihydroxybenzoic acid (DHBA), 2,6-DHBA, 3,5-DHBA, dihydrocaffeic acid (DHCA), 3-(2,4-dihydroxyphenyl)propionic acid (DHPPA), ellagic acid, enterodiol (EntD), enterolactone (EntL), gallic acid (GA), hippuric acid (HippurAc), homovanillic acid, 4-hydroxybenzoic acid (HBA), 3-hydroxyphenylacetic acid (HPAA), 3-(4-hydroxyphenyl)propionic acid (HPPA), phenylacetic acid (PAA), protocatechuic acid, pyrogallol, secoisolariciresinol, sinapic acid (SinapAc), urolithin (Uro) A, UroB, vanillic acid, and vanillin from Sigma-Aldrich (Steinheim, Germany); dihydroferulic acid (DHFA) from Alfa-Aesar (Haverhill, MA, USA); ρ-coumaric acid (ρ-CoumAc), (-)-epicatechin, ferulic acid (FA), 3-HBA, and syringic acid (SyrAc) from Fluka (St. Louis, MO, USA); and methyl gallate from Phytolab (Vestenbergsgreuth, Germany). Sigma-Aldrich (Steinheim, Germany) supplied the solvents.

2.2. Chestnut shells

Shells were kindly provided by Sortegel (Bragança, Portugal) in October 2018. CS were dehydrated at 40 °C for 24 h, ground to 1 mm particle size (Retsch ZM200 ultra-centrifugal grinder, Germany) and stored at room temperature in the dark.

2.3. Subcritical water extraction (SWE)

The SWE was performed at 220 °C and 40 bar, for 30 min, under continuous shaking (200 rpm), using a Parr Reactor (Series 4560, Parr Instrument Company, Moline, Illinois, USA) according to Pinto, Vieira et al. (Pinto, Vieira, et al., 2021). A solid-to-liquid ratio of 10 g:100 mL (*w/v*) was employed ($n = 3$). The extract was filtered, centrifuged at 10,000 *g* for 5 min (Sigma 3-30KS, Sigma, Germany), lyophilized (Telstar, Cryodos −80, Spain), and stored at 4 °C.

2.4. In-vivo studies

Male Wistar rats (200 ± 50 g, 5–6 weeks old) supplied by Jackson Laboratory (Bar Harbor, ME, USA) were acclimatized for 1 week, housed in polypropylene cages under standard conditions (temperature: 21 ± 2 °C; relative humidity: 45–55%; light/dark cycle: 12 h/12 h) and fed *ad libitum*. Animal procedures were performed as described by Pinto et al. (Pinto et al., 2023). The animals were randomly separated into three groups ($n = 6$ per group): a control group orally administered with water (4 mL/kg body weight (b.w.)) and two treatment groups orally treated with two doses of CS extract (50 and 100 mg/kg b.w.) dispersed in water. The solutions were administered *per os* by gastric gavage once daily, for 7 days, after a fasting period of 4 h. Acute toxicity test was

conducted to ascertain the toxic effects of the two doses of extract by examining the health status, body weight, and behavior. A minimum number of animals was used following a commitment to the 3R's policy (Replacement, Reduction & Refinement). All procedures were approved by the Local Ethical Committee from the Animal Welfare Body at i3S – Institute for Research & Innovation in Health (protocol number BSm_2017_10) and accomplished following FELASA, ARRIVE guidelines and European Directive 2010/63/EU for animal experiments. The general health status was monitored, and humane endpoints were defined in the case of any toxic effect and impairment of animal welfare. At the end of the experiments, the animals were euthanized by pentobarbital overdose (50 mg/kg b.w.).

2.4.1. Metabolomic profiling targeted on polyphenols

2.4.1.1. Preparation of extract. The extract (10 mg) was dissolved in 1 mL ice-cold acetonitrile (ACN) with 2% formic acid. Afterwards, 100 μL of solution was transferred to vials for analysis.

2.4.1.2. Tissues pre-treatment. Liver and kidneys of rats were dissected and handled on ice, in a room with light-filter. The tissue homogenates were prepared with 50 mM potassium phosphate (pH 7.0) at 1:5 (*w/v*) ratio, using a T10 basic Ultra-Turrax® (IKA laboratory technology, Staufen, Germany). After centrifuging at 20,000 *g* for 10 min (4 °C), the supernatants were kept at −80 °C. The protein precipitation was performed as described in previous studies (López-Yerena, Vallverdú-Queralt, et al., 2021; Pinto et al., 2023). Briefly, tissue homogenates were thawed and centrifuged at 11,000 *g* for 10 min (4 °C). The upper layer (100 μL) was added to ice-cold ACN with 2% formic acid in 1:4 (*v/v*) ratio. Preliminary tests were done to ascertain the most adequate ratio. Samples were homogenized for 1 min, stored at − 20 °C for 20 min, and centrifuged at 11,000 *g* for 10 min (4 °C). Finally, 100 μL of the organic phase was transferred to vials for analysis.

2.4.1.3. LC-ESI-LTQ-Orbitrap-MS analysis. Metabolomic studies were accomplished according to Escobar-Avelló et al. (Escobar-Avello et al., 2021), with minor modifications (Pinto et al., 2023), in LC-ESI-LTQ-Orbitrap-MS apparatus containing an Accela chromatograph (Thermo Scientific, Hemel Hempstead, UK) and equipped with a photodiode array detector, a quaternary pump, and a thermostated autosampler attached to an LTQ Orbitrap Velos mass spectrometer (Thermo Scientific, Hemel Hempstead, UK) with an ESI source in negative mode, using XCalibur v3.0 software (ThermoFisher Scientific, Hemel Hempstead, UK).

Chromatographic separation was performed using Acquity™ UPLC® BEH C_{18} Column (2.1 × 100 mm, i.d., 1.7 μm particle size) (Waters Corporation, Ireland) maintained at 30 °C. Mobile phases were water (A) and ACN (B) both with 0.1% formic acid. The solvent gradient (*v/v*) (t (min), %B) was applied as follows: (0, 0); (2, 0); (3, 30); (4, 100); (5, 100); (6, 0); (9, 0). Flow rate, injection volume and column temperature were set, respectively, at 0.450 mL/min, 5 μL, and 30 °C.

The instrumental conditions were set as described by Pinto et al. (Pinto et al., 2023). Samples were examined in full scan mode at a resolving power of 30,000 at *m/z* 600 and data-dependent MS/MS events were acquired at a resolving power of 15,000. Most intense ions were detected in FTMS mode triggered data-dependent scanning. Ions not sufficiently intense for a data-dependent scan were explored in MSn mode. Precursors were fragmented by collision-induced dissociation using a C-trap with normalized collision energy (35 V) and activation time of 10 ms.

The polyphenols were identified using commercial standards, whereas the identification of their metabolites was based on the elution time, chemical formula, and MS/MS fragmentation and compared to similar compounds. For the identification of phenolic metabolites in rat tissues, literature data and human metabolome database (https://hmdb.ca) were consulted. In the extract, the remaining compounds (of which the standards were not available) were identified by comparison with previous data from our research group (Escobar-Avello et al., 2021; Sasot et al., 2017), considering chemical formula, mass spectrometry fragmentation, and retention times, as well as confirmed through databases (https://foodb.ca and https://phenol-explorer.eu). Previous studies followed identical procedures for the identification of polyphenols in foods, plant extracts and biological tissues (Escobar-Avello et al., 2021; Sasot et al., 2017). MS^n patterns were acquired to determine the fragment ions produced in the linear ion trap. The elemental composition of the phenolic metabolites was assessed by accurate masses and isotopic patterns. In FTMS mode, the mass range was set from *m/z* 100 to 800.

The quantification of polyphenols and their metabolites was achieved by plotting the calibration curves in the respective tissues (concentration range = 0.1–3 μg/mL, $R^2 > 0.992$) for the polyphenols previously identified as major compounds in CS extract, prepared using the same extraction technique and conditions, i.e., GA, ellagic acid, methyl gallate, protocatechuic acid, and pyrogallol (Pinto, Vieira, et al., 2021). Semi-quantification was attained for the remaining polyphenols by comparison with the respective standards. The semi-quantification of phenolic metabolites was also performed by comparing with the standards of parent compounds through calibration curves plotted, owing to the lack of standards for phenolic metabolites available on the market. The use of the respective tissues (i.e., rat liver and kidney) to plot the calibration curves is of uttermost importance to eliminate interferences from matrix effects, providing the accurate identification and quantification of polyphenolics and their metabolites (López-Yerena, Domínguez-López, et al., 2021; López-Yerena, Vallverdú-Queralt, et al., 2021); Pinto et al., 2023). Besides identification, recent studies have successfully employed LC-ESI-LTQ-Orbitrap-MS for quantitative analysis targeted to polyphenols and their metabolites, using appropriate methods, databases, and standards for all compounds to be quantified, and applied to a high variety of complex samples, such as human and rat blood serum, human urine, rat organs (e.g., liver, kidney, intestine, lung, and heart), and rat tissues (e.g., muscle and skin), confirming its reproducibility and feasibility (Laveriano-Santos, Marhuenda-Muñoz, et al., 2022; Laveriano-Santos, Quifer-Rada, et al., 2022; (López-Yerena, Domínguez-López, et al., 2021; López-Yerena, Vallverdú-Queralt, et al., 2021); Pinto et al., 2023;Sasot et al., 2017). System control and data treatment were performed using XCalibur v3.0 software (ThermoFisher Scientific, Hemel Hempstead, UK). The results were expressed in nmol of each polyphenol equivalents per mg of tissue (nmol/g tissue).

2.5. Data statistics

The results were presented as mean ± SD of three independent experiments. IBM SPSS Statistics v24.0 software (Chicago, IL, USA) was used for one-way ANOVA and Tukey's HSD tests. A denoting significance was set for $p < 0.05$. Principal component analysis (PCA) and Pearson correlations between *in and vivo* antioxidant activity (data published in our previous paper (Pinto et al., 2023)) and metabolic profile of rat tissues were accomplished using GraphPad Prism v9 software (La Jolla, CA, USA). PCA was performed to allow the identification of variables that most significantly affect the samples clustering. Two principal components (PC) were used to establish the model after confirming the normal distribution of the variables. Prior to the PCA, an ANOVA analysis and a Bartlett's test for sphericity were carried out to ascertain all the assumptions needed for a suitable PCA application (Bailey, 2012; Spiegelberg & Rusz, 2017). A scores plot was designed to identify the trends among treatment groups, while a biplot diagram was used to disclose the contribution of different variables.

Table 1
Identification of phenolic compounds and their metabolites detected in liver and kidney tissues from rats orally treated with CS extract explored by LC-ESI-LTQ-Orbitrap-MS.

Compound	Neutral molecular formula	Rt (min)	Ion mass [M−H]⁻		Error (amu)	MS^2 fragment ions [M−H]⁻	Rat tissues		CS extract
			Theoretical	*Experimental*			Liver	Kidney	
Gallic acid-*O*-sulfate	$C_7H_6O_8S$	0.55	248.9711	248.9685	−1.4584	169.01206	−	+	−
Dimethyl-gallic acid-*O*-sulfate	$C_9H_{10}O_8S$	0.62	277.0024	276.9993	−1.9968	125.02406, 169.01225, 183.01558	+	+	−
Methyl-pyrogallol-*O*-sulfate	$C_7H_8O_6S$	0.73	218.9968	218.9963	0.5375	125.02416, 138.97908	−	+	−
Gallic acid	$C_7H_6O_5$	1.14	169.0142	169.0206	0.0075	125.02371	−	−	+
Dihydrogallic acid	$C_7H_8O_5$	1.68	171.0299	171.0292	0.004	127.03718, 141.01816	+	−	−
Pyrogallol	$C_6H_6O_3$	2.17	125.0244	125.0244	0.0010	81.03398, 97.02871	+	−	+
Dihydropyrogallol	$C_6H_8O_3$	2.71	127.0401	127.0359	−0.0031	125.02413	−	+	−
(Epi)catechin-*O*-glucuronide	$C_{21}H_{22}O_{12}$	4.30	465.1038	465.1023	−0.4966	179.03500, 245.11344, 289.06834	+	−	−
Protocatechuic acid-*O*-sulfate	$C_7H_6O_7S$	4.34	232.9761	232.9754	0.3837	109.02917, 153.01849	−	+	−
Catechol-*O*-sulfate	$C_6H_6O_5S$	4.47	188.9863	188.9860	0.7720	109.02921	+	+	−
Protocatechuic acid	$C_7H_6O_4$	4.48	153.0193	153.0194	0.0011	109.02860, 125.02344	+	+	+
Methyl-urolithin C-*O*-sulfate	$C_{14}H_{10}O_8S$	4.49	337.0024	337.0022	0.9024	199.00629, 243.02727	+	−	−
Urolithin A-*O*-sulfate	$C_{13}H_8O_7S$	4.50	306.9918	306.9912	0.5112	227.03806	+	+	−
Hydroxybenzoic acid-*O*-sulfate	$C_7H_6O_6S$	4.56	216.9812	216.9809	0.8022	121.02944, 137.02446	+	+	−
Dimethyl-pyrogallol-*O*-sulfate	$C_8H_{10}O_6S$	4.59	233.0125	233.0122	0.7848	125.02511, 139.03949, 153.01931	−	+	−
Protocatechuic acid-*O*-glucoside	$C_{13}H_{16}O_9$	4.61	315.0722	315.0702	−0.8375	109.02918, 153.01872	−	−	+
Methyl-protocatechuic acid-*O*-sulfate	$C_8H_8O_7S$	4.62	246.9918	246.9913	0.5875	109.02931, 153.01921, 232.97561	+	+	−
Dihydrocaffeic acid-*O*-sulfate	$C_9H_{10}O_7S$	4.64	261.0074	261.0070	0.6082	137.06062, 181.05060	−	+	−
Dimethyl-catechol-*O*-sulfate	$C_8H_{10}O_5S$	4.65	217.0176	217.0174	0.8592	109.02933, 123.04489	+	+	−
Pyrogallol-*O*-glucuronide	$C_{12}H_{14}O_9$	4.65	301.0565	301.0584	2.9737	125.02433	+	−	−
Dimethyl-urolithin C-*O*-sulfate	$C_{15}H_{12}O_8S$	4.67	351.0180	351.0178	0.8773	199.00651, 243.01742	+	−	−
Methyl-catechol	$C_7H_8O_2$	4.68	123.0452	123.0448	0.0007	109.02926	+	−	−
Caffeic acid-*O*-sulfate	$C_9H_8O_7S$	4.69	258.9918	258.9914	0.7244	135.04504, 179.03489	−	+	−
Catechol	$C_6H_6O_2$	4.70	109.0295	109.0302	0.0018	66.08643	+	+	−
Methyl-(epi)catechin	$C_{16}H_{16}O_6$	4.71	303.0874	303.0872	0.9046	179.05471, 289.07346	+	−	−
Hydroxyphenylacetic acid-*O*-sulfate	$C_8H_8O_6S$	4.72	230.9969	230.9966	0.7969	107.05001, 151.03999	−	+	−
Dihydroferulic acid-*O*-glucuronide	$C_{16}H_{20}O_{10}$	4.74	371.0984	371.1018	0.0045	151.03982, 195.06628	+	−	−
Dimethyl-syringic acid-*O*-sulfate	$C_{11}H_{14}O_8S$	4.75	305.0337	305.0331	0.5166	153.05548, 197.04302, 225.07685	+	+	−
Dimethyl-catechol	$C_8H_{10}O_2$	4.76	137.0608	137.0602	0.0005	109.02911, 123.04491	+	+	−
Sinapic acid-*O*-glucoside	$C_{17}H_{22}O_{10}$	4.76	385.1140	385.1128	−0.0002	223.06028	−	−	+
Catechol-*O*-glucuronide	$C_{12}H_{14}O_8$	4.77	285.0616	285.0633	0.0028	109.02917	+	+	−
Dihydroxyphenylpropionic acid	$C_9H_{10}O_4$	4.77	181.0506	181.0500	0.0004	137.02418	−	−	+
Chlorogenic acid	$C_{16}H_{18}O_9$	4.79	353.0878	353.0843	−0.0024	135.03072, 179.03406, 191.05512	+	−	+
Methyl gallate	$C_8H_8O_5$	4.80	183.0299	183.0291	−0.2759	125.02419, 169.01369	−	−	+
Coumaric acid-*O*-sulfate	$C_9H_8O_6S$	4.81	242.9969	242.9967	0.8732	119.04991, 163.03981	+	+	−
4-Hydroxybenzoic acid	$C_7H_6O_3$	4.82	137.0244	137.0242	0.9149	93.03389	−	+	+
Ferulic acid-*O*-sulfate	$C_{10}H_{10}O_7S$	4.83	273.0074	273.0072	0.8465	134.03508, 149.02383, 193.05076	−	+	−
Hydroxybenzoic acid-*O*-glucoside	$C_{13}H_{16}O_8$	4.83	299.0772	299.0767	0.0005	137.02418	−	−	+
Dihydroferulic acid-*O*-sulfate	$C_{10}H_{12}O_7S$	4.84	275.0231	275.0227	0.6747	195.06596	−	+	−
2,5-Dihydroxybenzoic acid	$C_7H_6O_4$	4.84	153.0193	153.0191	0.0008	109.02885	−	−	+
Coumaroylquinic acid	$C_{16}H_{18}O_8$	4.86	337.0929	337.0908	−0.010	163.03956, 191.07057	−	−	+
Hydroxyphenylpropionic acid-*O*-sulfate	$C_9H_{10}O_6S$	4.86	245.0125	245.0122	0.8024	121.02935, 165.05573	+	+	−
Methyl-coumaric acid-*O*-sulfate	$C_{10}H_{10}O_6S$	4.87	257.0125	257.0116	0.1920	119.04989, 163.03987, 177.05564	+	−	−
Methyl-catechol-*O*-sulfate	$C_7H_8O_5S$	4.88	203.0020	203.0017	0.8080	109.0293, 123.04492	−	+	−
Feruloylquinic acid	$C_{17}H_{20}O_9$	4.88	367.1035	367.1021	−0.0002	191.03418, 193.01396	−	−	+
Dihydrocaffeic acid	$C_9H_{10}O_4$	4.89	181.0506	181.0502	0.0007	137.06017	+	+	−
(Epi)catechin	$C_{15}H_{14}O_6$	4.91	289.0718	289.0709	0.0002	245.08078	−	−	+
Coumaric acid-*O*-glucoside	$C_{15}H_{18}O_8$	4.92	325.0928	325.0912	−0.5769	119.04954, 163.03961	−	−	+
Dicaffeoylquinic acid	$C_{25}H_{24}O_{12}$	4.92	515.1194	515.1175	−0.9098	173.08122, 191.03419, 335.07554, 353.08589	−	−	+
Hippuric acid	$C_9H_9NO_3$	4.93	178.0510	178.0512	1.3508	134.06059	+	+	−
Ferulic acid-*O*-glucoside	$C_{16}H_{20}O_9$	4.93	355.1035	355.1015	−0.8266	149.06000, 178.05833, 193.01380	−	−	+
Methyl-catechol-*O*-glucuronide	$C_{13}H_{16}O_8$	4.93	299.0772	299.0774	1.2487	109.02933, 123.04491	+	−	−
(Epi)gallocatechin-*O*-gallate	$C_{22}H_{18}O_{11}$	4.94	457.0776	457.0749	−1.6476	169.01339, 305.06491, 331.04429	−	−	+
Syringic acid	$C_9H_{10}O_5$	4.95	197.0455	197.0443	−0.1841	137.02383, 153.05535	+	+	+
(Epi)catechin-*O*-glucoside	$C_{21}H_{24}O_{11}$	4.96	451.1246	451.1224	−1.1124	245.07987, 289.07060	−	−	+
Methyl-dihydroferulic acid-*O*-sulfate	$C_{11}H_{14}O_7S$	4.97	289.0387	289.0384	0.7107	151.07650, 195.06564, 209.08016	−	+	−
3-Hydroxybenzoic acid	$C_7H_6O_3$	4.98	137.0244	137.0238	0.5137	93.03386	−	−	+
Urolithin B-*O*-sulfate	$C_{13}H_8O_6S$	4.98	290.9969	290.9955	−0.2407	211.03747	+	+	−
3-Hydroxyphenylacetic acid	$C_8H_8O_3$	4.99	151.0400	151.0398	0.8396	107.04999	−	+	−

(*continued on next page*)

Table 1 (*continued*)

Compound	Neutral molecular formula	Rt (min)	Ion mass [M−H]⁻		Error (amu)	MS² fragment ions [M−H]⁻	Rat tissues		CS extract
			Theoretical	*Experimental*			Liver	Kidney	
Caffeic acid-*O*-glucoside	$C_{15}H_{18}O_9$	5.00	341.0878	341.0859	−0.8015	135.04672, 179.03437	−	−	+
Ellagic acid	$C_{14}H_6O_8$	5.01	300.9989	300.9977	−0.1519	201.01796, 229.01404, 257.00856	+	−	+
Dimethyl-urolithin A	$C_{15}H_{12}O_4$	5.02	255.0663	255.0651	−0.0913	227.03805	+	−	−
Urolithin D	$C_{13}H_8O_6$	5.03	259.0248	259.0233	−0.4295	213.01692, 242.01543	+	+	−
Caffeic acid	$C_9H_8O_4$	5.04	179.0349	179.0343	0.4471	135.04466	+	−	+
Hydroxyphenylpropionic acid	$C_9H_{10}O_3$	5.05	165.0557	165.0553	0.7077	121.02926	+	+	+
Methyl-syringic acid	$C_{10}H_{12}O_5$	5.06	211.0612	211.0610	0.8894	137.06030, 153.05548, 197.04174	+	+	−
ρ-Coumaric acid	$C_9H_8O_3$	5.07	163.0400	163.0393	0.3055	119.04975	+	+	+
Syringic acid-*O*-glucoside	$C_{15}H_{20}O_{10}$	5.08	359.0983	359.0966	−0.6850	197.04472	−	−	+
Sinapic acid	$C_{11}H_{12}O_5$	5.09	223.0611	223.0603	0.2028	163.07562, 179.07061	+	+	+
Cinnamic acid-*O*-glucuronide	$C_{15}H_{16}O_8$	5.09	323.0772	323.0779	1.7675	147.04501	+	−	−
Enterodiol-*O*-sulfate	$C_{18}H_{22}O_7S$	5.09	381.1013	381.1007	0.4884	301.13897	−	+	−
2,6-Dihydroxybenzoic acid	$C_7H_6O_4$	5.10	153.0193	153.0186	0.3501	109.02893	−	−	+
Dihydroferulic acid	$C_{10}H_{12}O_4$	5.11	195.0662	195.0663	1.0836	135.04459, 151.07562	+	+	−
Dimethyl-ellagic acid	$C_{16}H_{10}O_8$	5.11	329.0303	329.0272	−1.9720	300.99997	+	−	−
Ferulic acid	$C_{10}H_{10}O_4$	5.12	193.0506	193.0501	0.5288	135.04437, 149.06049, 179.03409	−	−	+
Enterolactone-*O*-glucuronide	$C_{24}H_{26}O_{10}$	5.12	473.1453	473.1452	0.9488	297.11531	−	+	−
Methyl-ferulic acid-*O*-sulfate	$C_{11}H_{12}O_7S$	5.13	287.0231	287.0225	0.4916	149.06051, 193.05064, 207.06135	−	+	−
Dihydrocaffeic acid-*O*-glucuronide	$C_{15}H_{18}O_{10}$	5.14	357.0827	357.0815	−0.0801	137.06066, 181.05055	+	+	−
m-Coumaric acid	$C_9H_8O_3$	5.14	163.0400	163.0395	0.5191	119.04948	−	−	+
Sinapic acid-*O*-sulfate	$C_{11}H_{12}O_8S$	5.15	303.0180	303.0174	0.5111	223.06104	−	+	−
(Epi)catechin-*O*-gallate	$C_{22}H_{18}O_{10}$	5.16	441.0827	441.0815	−0.1717	169.01340, 271.06002, 289.07060, 331.04445	−	−	+
Urolithin C	$C_{13}H_8O_5$	5.17	243.0299	243.0271	−1.7460	185.01711, 199.04242	+	+	−
Methyl-dihydroferulic acid	$C_{11}H_{14}O_4$	5.18	209.0819	209.0794	−1.4134	151.03962, 193.04991, 195.06308	−	+	−
o-Coumaric acid	$C_9H_8O_3$	5.22	163.0400	163.0393	0.3208	119.04980	−	−	+
(Epi)gallocatechin	$C_{15}H_{14}O_7$	5.24	305.0667	305.0656	0.0336	179.03423, 219.06537, 221.04437, 261.07572	−	−	+
Enterodiol	$C_{18}H_{22}O_4$	5.24	301.1445	301.1425	−0.8880	271.13314	+	−	−
Secoisolariciresinol	$C_{20}H_{26}O_6$	5.25	361.1657	361.1648	0.1995	151.03954, 165.05508, 346.14081	+	−	+
Hydroxyphenylacetic acid-*O*-glucuronide	$C_{14}H_{16}O_9$	5.26	327.0722	327.0718	0.7189	151.03983	+	−	−
Urolithin A	$C_{13}H_8O_4$	5.27	227.0349	227.0342	0.2945	183.04514	−	+	−
Enterolactone-*O*-sulfate	$C_{18}H_{18}O_7S$	5.28	377.0700	377.0697	0.7216	297.11274	+	+	−
Enterolactone-*O*-disulfate	$C_{18}H_{18}O_{10}S_2$	5.32	457.0269	457.0257	−0.0382	297.11398, 377.06977	−	+	−
Methyl-urolithin B	$C_{14}H_{10}O_3$	5.37	225.0557	225.0533	−1.3675	211.03746	−	+	−
3-Phenylpropionic acid	$C_9H_{10}O_2$	5.38	149.0608	149.0600	0.3067	105.06998	−	−	+
Cinnamic acid	$C_9H_8O_2$	5.39	147.0452	147.0444	0.3165	102.94863	+	−	+
Enterolactone	$C_{18}H_{18}O_4$	5.40	297.1132	297.1128	0.6269	107.04977, 217.04738, 253.12255	+	+	−
Hydroxyphenylpropionic acid-*O*-glucuronide-sulfate	$C_{15}H_{18}O_{12}S$	5.63	421.0446	421.0460	2.4975	121.02967, 165.05579, 341.07019	+	+	−
Dimethyl-urolithin B	$C_{15}H_{12}O_3$	5.87	239.0714	239.0713	1.0489	211.03259	+	−	−

+, compound identified in samples; −, compound not identified in samples.

3. Results and discussion

3.1. Metabolomic profiling of chestnut shells extract

Plant-based foods and their by-products have been indicated as vital allies in the promotion of a healthy lifestyle by preventing chronic diseases, protecting against premature aging, and providing many other health benefits (Rudrapal et al., 2022). A comprehensive assessment of the biological effects of plant-based foods depends not only on their nutritional and phytochemical composition, but also on an in-depth understanding of their metabolism and *in-vivo* bioactivity (Martins et al., 2016; Rudrapal et al., 2022). Most of the pro-healthy properties of plant-based foods, such as CS, are attributed to their richness in polyphenols (Lameirão et al., 2020; Pinto & Cádiz-Gurrea et al., 2020; Pinto, Silva, et al., 2021; Pinto, Vieira, et al., 2021).

Recently, our research group performed a preliminary study on the phytochemical composition of the CS extract prepared using the same extraction technology and conditions by LC/ESI-MS and reported its richness in ellagic acid, GA, protocatechuic acid, methyl gallate, and pyrogallol (Pinto, Vieira, et al., 2021). Nonetheless, several compounds remained unknown. This study evaluated the full metabolomic profiling of CS extract targeted on polyphenols, especially considering the ones already identified in the previous study. Notwithstanding, a comprehensive examination regarding the unknown compounds was also performed before the metabolomic approach in liver and kidney. Table 1 presents the polyphenols and metabolites identified in CS extract and rat tissues. Fig. 1 depicts the polyphenols quantified in CS extract.

A total of 37 compounds were identified in the extract, with a total content of 107.80 μmol/g dw. The different polyphenolic classes are present in the following order: phenolic acids (89.31%) > tannins (2.38%) > flavonoids (0.88%). Among phenolic acids, hydroxybenzoic acids (HBAs) represent 57.74% of the total content, while 30.04% correspond to hydroxycinnamic acids (HCAs). A small amount of hydroxyphenylpropanoic acids (HPPAs) (1.53%) was also detected. Protocatechuic acid (48.47 μmol/g dw) was the major compound identified, followed by CinnamAc (22.38 μmol/g dw), 4-HBA (11.32 μmol/g dw), and pyrogallol (10.09 μmol/g dw). Some of these compounds may result from the thermal degradation of more complex

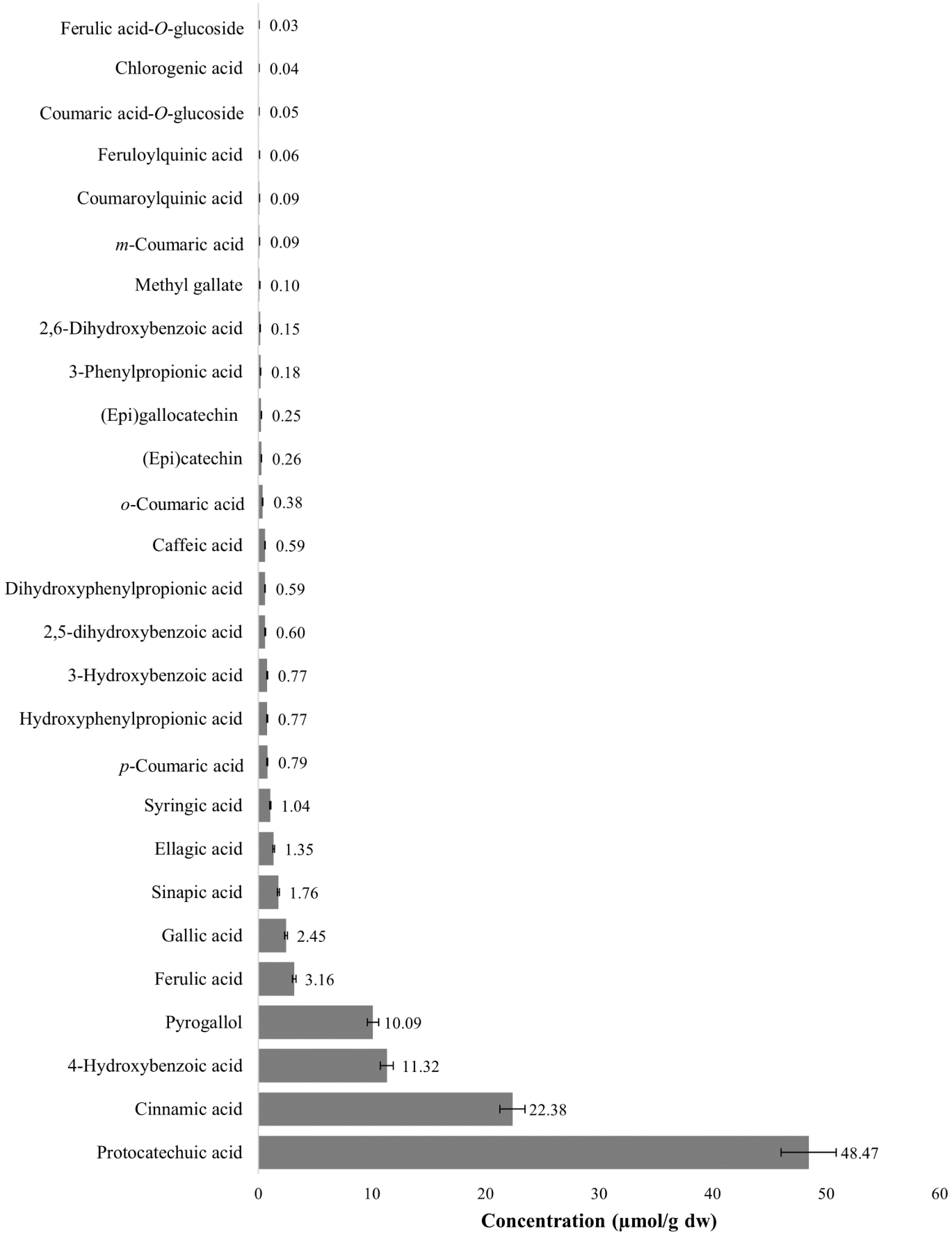

Fig. 1. Quantification of phenolic compounds in chestnut shells extract explored by LC-ESI-LTQ-Orbitrap-MS.

Table 2
Quantification of phenolic compounds and their metabolites in liver and kidney tissues from rats orally treated with water (control group), 50 mg/kg b.w. and 100 mg/kg b.w. of CS extract explored by LC-ESI-LTQ-Orbitrap-MS.

Phenolic compounds and metabolites	Concentration (nmol/g tissue) Liver			Kidney		
	Control (water)	CS extract 50 mg/kg b.w.	CS extract 100 mg/kg b.w.	Control (water)	CS extract 50 mg/kg b.w.	CS extract 100 mg/kg b.w.
Phenolic acids – Hydroxybenzoic acids						
Dihydrogallic acid	n.i.	1.18 ± 0.16^{a}	0.95 ± 0.12^{b}	n.i.	n.i.	n.i.
Gallic acid-*O*-sulfate	n.i.	n.i.	n.i.	n.i.	0.32 ± 0.02^{a}	0.32 ± 0.03^{a}
Dimethyl-gallic acid-*O*-sulfate	n.i.	$1.05 \pm 0.15^{b,1}$	$1.20 \pm 0.22^{a,1}$	n.i.	$0.38 \pm 0.09^{a,2}$	$0.36 \pm 0.05^{a,2}$
Methyl-syringic acid	n.i.	$1.67 \pm 0.25^{a,2}$	$1.78 \pm 0.46^{a,2}$	n.i.	$3.59 \pm 0.76^{a,1}$	$2.55 \pm 0.56^{b,1}$
Dimethyl-syringic acid-*O*-sulfate	n.i.	n.q.	n.q.	n.i.	3.96 ± 0.94^{b}	6.59 ± 1.85^{a}
4-Hydroxybenzoic acid	n.i.	n.i.	n.i.	n.i.	1.84 ± 0.48^{a}	1.79 ± 0.49^{a}
Hydroxybenzoic acid-*O*-sulfate	n.i.	n.q.	n.q.	n.i.	211.53 ± 63.16^{a}	228.41 ± 57.02^{a}
Hippuric acid	$29.96 \pm 0.25^{b,2}$	$77.88 \pm 13.88^{a,2}$	$68.94 \pm 14.15^{a,2}$	$59.77 \pm 12.12^{b,1}$	$205.18 \pm 43.65^{a,1}$	$171.54 \pm 49.72^{a,1}$
Phenolic acids – Hydroxycinnamic acids						
Caffeic acid	n.i.	0.05 ± 0.01^{b}	0.07 ± 0.01^{a}	n.i.	n.i.	n.i.
Caffeic acid-*O*-sulfate	n.i.	n.i.	n.i.	n.i.	1.17 ± 0.21^{b}	1.33 ± 0.33^{a}
Dihydrocaffeic acid	n.i.	$1.39 \pm 0.25^{b,1}$	$1.62 \pm 0.33^{a,1}$	n.i.	$0.30 \pm 0.05^{a,2}$	$0.31 \pm 0.04^{a,2}$
Dihydrocaffeic acid-*O*-glucuronide	n.i.	0.31 ± 0.06^{a}	0.32 ± 0.05^{a}	n.i.	n.q.	n.q.
Dihydrocaffeic acid-*O*-sulfate	n.i.	n.i.	n.i.	n.i.	10.64 ± 2.37^{a}	7.01 ± 1.78^{b}
Ferulic acid-*O*-sulfate	n.i.	n.i.	n.i.	n.i.	34.04 ± 7.20^{b}	41.48 ± 9.02^{a}
Dihydroferulic acid	n.i.	$0.54 \pm 0.09^{a,2}$	$0.49 \pm 0.08^{a,2}$	n.i.	$1.08 \pm 0.23^{a,1}$	$1.01 \pm 0.26^{a,1}$
Dihydroferulic acid-*O*-glucuronide	n.i.	0.16 ± 0.03^{b}	0.23 ± 0.04^{a}	n.i.	n.i.	n.i.
Dihydroferulic acid-*O*-sulfate	n.i.	n.i.	n.i.	n.i.	15.16 ± 2.89^{b}	20.16 ± 4.19^{a}
Methyl-dihydroferulic acid-*O*-sulfate	n.i.	n.i.	n.i.	n.i.	1.72 ± 0.48^{a}	1.43 ± 0.39^{a}
p-Coumaric acid	n.i.	$0.47 \pm 0.08^{a,2}$	$0.43 \pm 0.06^{a,2}$	n.i.	$3.90 \pm 1.18^{a,1}$	$3.97 \pm 1.12^{a,1}$
Coumaric acid-*O*-sulfate	n.i.	n.q.	n.q.	n.i.	3.91 ± 0.94^{a}	3.05 ± 0.66^{b}
Cinnamic acid	n.i.	471.09 ± 84.28^{a}	508.45 ± 90.04^{a}	n.i.	n.i.	n.i.
Cinnamic acid-*O*-glucuronide	n.i.	8.76 ± 2.25^{a}	7.45 ± 1.79^{a}	n.i.	n.i.	n.i.
Sinapic acid-*O*-sulfate	n.i.	n.i.	n.i.	n.i.	1.04 ± 0.25^{a}	0.76 ± 0.20^{b}
Phenolic acids - Hydroxyphenylacetic acids						
Hydroxyphenylacetic acid	n.i.	n.i.	n.i.	n.i.	68.92 ± 12.20^{a}	69.09 ± 7.74^{a}
Hydroxyphenylacetic acid-*O*-glucuronide	n.i.	0.76 ± 0.19^{a}	0.84 ± 0.17^{a}	n.i.	n.i.	n.i.
Hydroxyphenylacetic acid-*O*-sulfate	n.i.	n.i.	n.i.	n.i.	44.68 ± 10.45^{a}	39.63 ± 10.63^{a}
Phenolic acids - Hydroxyphenylpropanoic acids						
Hydroxyphenylpropionic acid	n.i.	$114.53 \pm 22.36^{a,2}$	$94.82 \pm 23.24^{b,2}$	n.i.	$739.48 \pm 131.03^{b,1}$	$870.47 \pm 176.75^{a,1}$
Hydroxyphenylpropionic acid-*O*-sulfate	n.i.	$242.83 \pm 34.78^{a,2}$	$226.79 \pm 56.13^{a,2}$	n.i.	$1319.31 \pm 323.23^{a,1}$	$1572.23 \pm 440.96^{a,1}$
Hydroxyphenylpropionic acid-*O*-glucuronide-sulfate	n.i.	19.18 ± 2.93^{a}	19.59 ± 2.76^{a}	n.i.	n.q.	n.q.
Flavonoids						
(Epi)catechin-*O*-glucuronide	n.i.	0.09 ± 0.01^{a}	0.10 ± 0.02^{a}	n.i.	n.i.	n.i.
Methyl-(epi)catechin	n.i.	0.08 ± 0.02^{a}	0.07 ± 0.02^{a}	n.i.	n.i.	n.i.
Lignans metabolites						
Enterodiol	n.i.	0.08 ± 0.02^{a}	0.13 ± 0.02^{b}	n.i.	n.i.	n.i.
Enterolactone	n.i.	0.31 ± 0.05^{a}	0.28 ± 0.04^{a}	n.i.	n.q.	n.q.
Enterolactone-*O*-sulfate	n.i.	$0.92 \pm 0.21^{a,1}$	$0.71 \pm 0.11^{b,1}$	n.i.	$0.24 \pm 0.05^{b,2}$	$0.30 \pm 0.05^{a,2}$
Enterolactone-*O*-disulfate	n.i.	n.i.	n.i.	n.i.	0.66 ± 0.04^{a}	0.64 ± 0.04^{a}
Hydrolysable tannins metabolites						
Urolithin A-*O*-sulfate	n.i.	$2.75 \pm 0.44^{a,1}$	$2.59 \pm 0.49^{a,1}$	n.i.	$1.46 \pm 0.27^{a,2}$	$1.44 \pm 0.18^{a,2}$
Urolithin B-*O*-sulfate	n.i.	0.10 ± 0.02^{a}	0.11 ± 0.02^{a}	n.i.	n.q.	n.q.
Methyl-urolithin B	n.i.	n.i.	n.i.	n.i.	0.19 ± 0.05^{a}	0.15 ± 0.03^{b}
Dimethyl-urolithin B	n.i.	0.27 ± 0.05^{b}	0.33 ± 0.06^{a}	n.i.	n.i.	n.i.
Urolithin C	n.i.	$1.77 \pm 0.32^{a,1}$	$1.86 \pm 0.35^{a,1}$	n.i.	$1.93 \pm 0.49^{a,1}$	$1.28 \pm 0.29^{b,2}$
Methyl-urolithin C-*O*-sulfate	n.i.	0.08 ± 0.02^{a}	0.09 ± 0.01^{a}	n.i.	n.i.	n.i.
Urolithin D	n.i.	$4.32 \pm 0.89^{b,1}$	$5.95 \pm 1.23^{a,1}$	n.i.	$1.15 \pm 0.26^{a,2}$	$0.94 \pm 0.18^{b,2}$
Other polyphenols						
Catechol	n.i.	$0.53 \pm 0.12^{a,2}$	$0.56 \pm 0.10^{a,2}$	n.i.	$2.15 \pm 0.56^{a,1}$	$1.18 \pm 0.33^{b,1}$
Catechol-*O*-glucuronide	n.i.	0.10 ± 0.02^{a}	0.10 ± 0.02^{a}	n.i.	n.q.	n.q.
Catechol-*O*-sulfate	n.i.	n.q.	n.q.	n.i.	9.57 ± 2.27^{a}	9.29 ± 2.21^{a}
Methyl-catechol-*O*-sulfate	n.i.	n.i.	n.i.	n.i.	1.18 ± 0.28^{a}	1.05 ± 0.27^{a}
Dimethyl-catechol	n.i.	n.q.	n.q.	n.i.	1.05 ± 0.29^{a}	0.75 ± 0.06^{b}
Dimethyl-catechol-*O*-sulfate	n.i.	n.q.	n.q.	n.i.	0.70 ± 0.14^{a}	0.76 ± 0.21^{a}
Dihydropyrogallol	n.i.	n.i.	n.i.	n.i.	62.48 ± 8.91^{a}	57.61 ± 8.62^{b}

n.i., non-identified. n.q., non-quantified. Results are expressed as mean ± standard deviation, $n = 6$ in each group. Different letters (a and b) in the same line within the same rat tissue indicate significant differences between groups ($p < 0.05$). Different superscript numbers (1 and 2) in the same line within the same treatment group indicate significant differences between rat tissues ($p < 0.05$).

phenolic acids and flavonoids during the extraction at high temperatures (220 °C/30 min) (Pinto, Vieira, et al., 2021). For instance, pyrogallol may be generated via decarboxylation of GA, while protocatechuic acid is a catechin metabolite formed by its thermal decomposition (Bento-Silva et al., 2020). Ellagic acid was the only hydrolysable tannin identified, probably derived from ellagitannins degradation (Tomás-Barberán et al., 2014). Only two flavonoids were detected, (epi)catechin and (epi)gallocatechin, whose presence may be explained by the thermal decomposition of (epi)catechin-*O*-gallate and (epi)gallocatechin-*O*-gallate through the loss of GA. Secoisolariciresinol was the only lignan

detected.

Furthermore, phenolic glycosides derived from CA, CoumAc, (epi) catechin, FA, HBA, protocatechuic acid, SinapAc and SyrAc were identified. Due to the low quantities of these compounds, it was only possible to quantify FA-*O*-glucoside (0.03 μmol/g dw) and CoumAc-*O*-glucoside (0.05 μmol/g dw). The phenolic-derived glycosides may be decomposed into their parent compounds by the loss of glucose (Sasot et al., 2017). Trace contents of two quinic acids derivatives were also detected with 0.06 and 0.09 μmol/g dw of feruloylquinic and coumaroylquinic acids, respectively. These compounds may further lose quinic acid moieties, producing their parent compounds, namely FA and CoumAc (Sasot et al., 2017). Previous studies described similar phenolic profiles for eco-friendly CS extracts prepared by conventional extraction (Rodrigues et al., 2015) and green technologies, i.e., ultrasound-assisted extraction (Lameirão et al., 2020), supercritical fluid extraction (Pinto & Cádiz-Gurrea et al., 2020), and microwave-assisted extraction (Pinto, Silva, et al., 2021).

The use of polyphenols as key ingredients for adjuvant therapy of numerous lifestyle-related chronic diseases has been targeted on latest studies (Martins et al., 2016). Recent advances suggested that phenolic acids, including HCAs and HBAs, may serve as valuable molecules for the treatment of oxidative stress-related cardiovascular diseases, such as atherosclerosis, coronary heart disease, dyslipidemia, hypertension, stroke, and cancer, due to their strong antioxidant potential, protective effects against oxidative damage and signaling pathways modulation (Rudrapal et al., 2022). Beyond the antioxidant and antiradical properties, HCAs are natural molecules used in the management of lipid metabolism, obesity, and inflammatory metabolic diseases, i.e., CA, FA, *p*-CoumAc, ChlorogenAc and CinnamAc, via i) inhibiting the macrophage infiltration and nuclear factor κB (NF-κB) activation in adipose tissues; ii) preventing the expression of proinflammatory adipokines tumor necrosis factor-α (TNF-α), monocyte chemoattractant protein-1 (MCP-1), and plasminogen activator inhibitor type-1 (PAI-1); and iii) promoting the secretion of adiponectin capable of regulating the glucose levels, lipid metabolism, and insulin sensitivity owing to its anti-fibrotic, anti-inflammatory, and antioxidant effects (Alam et al., 2016). Therefore, polyphenols are potential candidates for the development of novel nutraceuticals with potential use in chronic pathologies.

3.2. Metabolomic fingerprinting in rat tissues

3.2.1. Identification and quantification of polyphenols and metabolites in the liver

Metabolomics combines high-throughput analytical methodologies and statistics to characterize the metabolic profiling of bioactive compounds and its effects on bioactivity, providing new insights into mechanisms of action and proposing novel biomarkers for the proven effects (López-Yerena, Domínguez-López, et al., 2021); Rudrapal et al., 2022). Several studies applied metabolomic approaches in blood or urine (López-Yerena, Domínguez-López, et al., 2021); Rudrapal et al., 2022; Sasot et al., 2017), however, just few studies have explored the metabolic profile in biological tissues (Anallely López-Yerena et al., 2021). In this regard, there is only one study evaluating the metabolomic profiling of blood serum from rats orally treated with CS extract (Pinto et al., 2023). Noteworthy, this is the first study that provides a comprehensive assessment of the metabolomic profile of tissues from rats orally treated with CS extract and correlate it with previously published outcomes of the *in-vivo* protective effects against oxidative stress.

All metabolites from the parent compounds identified in CS extract were searched in rat tissues. A total of 50 compounds were identified in the liver (Table 1). Beyond phenolic acids that represented 65% of the compounds detected, one lignan and three metabolites, two flavonoid metabolites, and one hydrolysable tannin, along with nine metabolites, were also present. The phenolic acids identified are generally weak basic molecules with low molecular weight (<250 g/mol) and mild lipophilicity (log P ~ 0.9), facilitating their absorption through passive transport (López-Yerena, Domínguez-López, et al., 2021); Pinto et al., 2023). The detection of unmetabolized compounds in liver and kidney tissues confirmed their absorption by passive diffusion or through carriers located in the intestine, while phase II metabolites were secreted owing to their high polarity and molecular weight (Marhuenda-Muñoz et al., 2019; Pinto et al., 2023). Almost 81% of the metabolites derived from phase II reactions, whereas 11% represent microbiota metabolites and the remaining 8% resulted from other phase I reactions. Furthermore, twelve compounds identified are parent compounds, while the remaining represent their metabolites. Considering HBAs, eight compounds were detected in liver. Although GA was not identified, two metabolites from phase I (hydrogenation) and II reactions (methylation and sulfation) were found. Likewise, Bhat et al. (Bhat et al., 2020) also reported dihydro-GA in rice bran. Unmetabolized SyrAc and two phase II metabolites from methylation and sulfation, as well as the sulfated conjugate of HBA, were detected. A fraction of protocatechuic acid reached the liver unchanged, along with its methylated and sulfated conjugates. HippurAc was also detected in liver.

Regarding HCAs, twelve compounds were identified. Small fractions of unmetabolized CA and *ρ*-CoumAc reached the liver, while FA was not detected. The phase I metabolites of CA and FA obtained by hydrogenation, DHCA and DHFA, were also identified, along with glucuronidated conjugates. Unmetabolized SinapAc and ChlorogenAc and two phase II metabolites of *ρ*-CoumAc were detected. A major fraction of unmetabolized CinnamAc accumulated in the liver, along with its glucuronidated conjugate.

Unmetabolized HPPA also reached the liver, along with sulfated and glucuronidated-sulfated conjugates, while HPAA-*O*-glucuronide was the only HPAA metabolite identified.

A small fraction of unmetabolized ellagic acid also reached the liver, along with its dimethylated conjugate and urolithins which are gut microbiota metabolites of ellagic acid (Tomás-Barberán et al., 2014). UroC and UroD were identified accompanied by methylated-sulfated and dimethylated-sulfated conjugates of UroC. Sulfated and methylated metabolites of UroA and UroB were also found.

Regarding lignans, secoisolariciresinol and three microbial metabolites (i.e., EntD, EntL, and EntL-*O*-sulfate) were the only compounds noticed.

Unlike the CS extract, epi(gallo)catechins and derivatives were not present in the liver, probably due to their high excretion and poor absorption rates (López-Yerena, Domínguez-López, et al., 2021). Only two-phase II metabolites of catechin were detected in liver.

Catechol was also found in liver, along with its methylated, sulfated and glucuronidated conjugates. A trace fraction of unmetabolized pyrogallol reached the liver, together with its glucuronidated conjugate.

Nonetheless, it was only possible to quantify some phenolic metabolites owing to their low concentrations, which hinders their quantification. Table 2 summarizes the polyphenols and metabolites quantified in rat tissues.

HCAs and HPPAs are the main classes of polyphenols and their circulating metabolites in the liver of CS extract-treated rats. CinnamAc was the major polyphenol identified (471.09 and 508.45 nmol/g tissue for 50 and 100 mg/kg b.w., respectively), followed by HPPA (114.53 and 94.82 nmol/g tissue). Furthermore, HPPA-*O*-sulfate was the main metabolite (242.83 and 226.79 nmol/g tissue), followed by HPPA-*O*-glucuronide-sulfate (19.18 and 19.59 nmol/g tissue) and CinnamAc-*O*-glucuronide (8.76 and 7.45 nmol/g tissue). Among HBAs, only two GA and one SyrAc metabolites were quantified. Even though HippurAc was the only metabolite quantified in control (29.96 nmol/g tissue), only trace levels ($p < 0.05$) were determined compared to treatment groups (77.88 and 68.94 nmol/g tissue, respectively, for 50 and 100 mg/kg b.w.). HippurAc is an endogenous metabolite found after the consumption of whole grains, cereals, and vegetable oils (Luzardo-Ocampo et al., 2017). This may explain its presence in the control group since rats fed a standard pellet diet composed by corn starch and soybean oil that may

be rich in polyphenols, mainly phenolic acids. Thus, HippurAc may also result, in a lower extent, from the metabolization of these phenolic acids into benzoic acid by phase I enzymes, with further conjugation with glycine (endogenously produced from amino acids delivered by diet) (Luzardo-Ocampo et al., 2017).

Considering HCAs, the highest levels correspond to CinnamAc metabolites (479.85 and 515.90 nmol/g tissue, respectively, for 50 and 100 mg/kg b.w.). CA metabolites represent 1.75–2.01 nmol/g tissue, while FA metabolites correspond to 0.70–0.72 nmol/g tissue, achieving both higher concentrations in the livers from 100 mg/kg b.w. CS extract-treated rats. Otherwise, similar contents of ρ-CoumAc and HPAA-*O*-glucuronide were determined in both groups. Metabolites from flavonoids and catechol corresponded to 0.17 and 0.65 nmol/g tissue, respectively. Ellagic acid metabolites were quantified in the following increasing concentrations: methyl-UroC-*O*-sulfate < UroB-*O*-sulfate < dimethyl-UroB < UroC < UroA-*O*-sulfate < UroD, with a total content of 9.29 and 10.93 nmol/g tissue for 50 and 100 mg/kg b.w. groups, respectively. The major metabolite of secoisolariciresinol in liver was EntL-*O*-sulfate (70%), followed by EntL (24%) and EntD (6%). In summary, higher concentrations of HCAs (519.06 nmol/g tissue), HPAAs (0.84 nmol/g tissue), ellagic acid metabolites (10.93 nmol/g tissue), and catechol metabolites (0.66 nmol/g tissue) were determined in liver from 100 mg/kg b.w. CS extract group. Otherwise, liver from 50 mg/kg b.w. CS extract group contained higher levels of HBAs (81.78 nmol/g tissue), HPPAs (376.54 nmol/g tissue), and lignans metabolites (1.31 nmol/g tissue). Similar concentrations of phenolic metabolites were determined in liver from rats treated with both extract doses, pointing out identical metabolomic profiles, which corroborate the similar *in-vivo* antioxidant effects attested in both treatment groups considering our previous study (Pinto et al., 2023).

Comparing to previous studies, Li et al. (Li et al., 2016) reported an identical metabolomic profile of Chinese water chestnut, including CA, FA, CinnamAc, ChlorogenAc, PAA, quinic acid, gallocatechin-7,4′-di-*O*-gallate, and epigallocatechin-5,7-di-*O*-gallate. Recently, Tu et al. (Tu et al., 2021) also described a similar metabolomic profiling of liver and intestine from rats orally treated with *Sanguisorba officinalis* tannins (150 mg/kg b.w.), underlining the presence of GA, (di)methyl-GA, pyrogallol, methyl-GA-*O*-glucuronide, methylated and sulfated UroA, and methyl-UroC in intestine, while only GA, (di)methyl-GA, ellagic acid and methyl-ellagic acid were found in liver. According to Llorach et al. (Llorach et al., 2010), the main urinary metabolites identified after a single intake of 3.5 g of almond shells extract were (epi)catechin sulfated and methylated conjugates, phenylvalerolactones (PVL) and phenylvaleric acids (PVA) metabolites, sulfated and glucuronidated conjugates of HPAAs and HPPAs, hydroxy-HippurAc and FA-*O*-glucuronide.

3.2.2. Identification and quantification of polyphenols and metabolites in the kidney

A total of 50 compounds were identified in kidney, with phenolic acids and their metabolites representing the major polyphenolic class (Table 1). Five lignans and six ellagic acid metabolites were also detected. Almost 83% of the metabolites are phase II metabolites, while 10% correspond to microbiota metabolites and the remaining 7% to other phase I metabolites. Only nine compounds identified are parent compounds, while the remaining correspond to their metabolites. Concerning HBAs, ten compounds were identified. As proven for the liver, GA was also not noticed in the kidney. Only GA methylated and sulfated conjugates were found. Dihydro-GA was not detected in kidney, oppositely to liver. Unmetabolized 4-HBA, protocatechuic acid, and SyrAc reached the kidney, corroborating that a considerable fraction of these phenolic acids from the CS extract remained unchanged, being capable of exerting their pro-healthy effects *in-vivo* without structural modifications on their molecules. Methylated and sulfated conjugates of HBA, protocatechuic acid, and SyrAc also accumulated in the kidney. Similar to liver, HippurAc was also detected in the kidney.

Among HCAs, fourteen compounds were identified, with 71% representing CA and FA metabolites, including phase I (DHCA and DHFA) and phase II conjugates (sulfated, methylated and, in a lower extent, glucuronidated). Unmetabolized CA and FA were not detected, in contrast to unmetabolized ρ-CoumAc and SinapAc that accumulated in the kidney along with their sulfated conjugates. Unlike liver, CinnamAc and ChlorogenAc were not detected in kidney, having probably been metabolized into simpler phenolic acids or formed conjugates.

As stated for liver, unmetabolized HPPA and its sulfated and glucuronidated-sulfated conjugates also accumulated in kidney. HPAA-*O*-sulfate was also found, accompanied by a higher fraction of its unmetabolized form. Unlike liver, no catechin metabolites were identified in kidney.

In contrast to liver, ellagic acid did not reach kidney. However, UroA, UroC, UroD, and methyl-UroB, and sulfated conjugates of UroA and UroB accumulated in kidney.

EntL and its phase II conjugates were the main lignan metabolites identified, together with EntD-*O*-sulfate.

Unmetabolized catechol accumulated in kidney, along with its methylated, sulfated and glucuronidated conjugates. Pyrogallol was not detected in its unmetabolized form, in contrast to liver. Nevertheless, dihydropyrogallol (not present in liver) was noticed in kidney, suggesting that a fraction of pyrogallol was metabolized by phase I enzymes. Pyrogallol conjugates arising from methylation and sulfation were also detected.

As shown in Table 2, HPPAs was the most representative polyphenolic class in kidney, representing 75 and 78% of total content, respectively, in 50 and 100 mg/kg b.w. groups, followed by HBAs (13 and 16%) and HPAAs (3.5 and 4%). HPPA was the main polyphenol quantified (739.48 and 870.47 nmol/g tissue, respectively, for 50 and 100 mg/kg b.w. groups), followed by HippurAc (205.18 and 171.54 nmol/g tissue). Regarding metabolites, HPPA-*O*-sulfate (1319.31 and 1572.23 nmol/g tissue) and HBA-*O*-sulfate (211.53 and 228.41 nmol/g tissue) were the main phase II conjugates, while dihydropyrogallol was the principal phase I metabolite (62.48 and 57.61 nmol/g tissue). Among HBAs, only sulfated and methylated conjugates from GA and SyrAc were quantified, with concentrations varying between 0.32 and 6.59 nmol/g tissue. Similar contents ($p > 0.05$) of GA metabolites, 4-HBA, HBA-*O*-sulfate, and HippurAc were determined in both groups. As ascertained in liver, HippurAc was the only metabolite in the control group (59.77 nmol/g tissue), although only trace levels ($p < 0.05$) were quantified when compared to CS extract groups (205.18 and 171.54 nmol/g tissue for 50 and 100 mg/kg b.w. groups). Ten HCAs metabolites were quantified in kidney, with concentrations increasing in the following order: DHCA < SinapAc-*O*-sulfate < DHFA < CA-*O*-sulfate < methyl-DHFA-*O*-sulfate < CoumAc-*O*-sulfate < *p*-CoumAc < DHCA-*O*-sulfate < DHFA-*O*-sulfate < FA-*O*-sulfate, in a total of 80 nmol/g tissue. High concentrations of unmetabolized HPPA and HPAA reached kidney, along with their sulfated metabolites, representing 2250 and 110 nmol/g tissue, respectively. Urolithins arouse as ellagic acid metabolites, with concentrations increasing as follows: methyl-UroB < UroD < UroA-*O*-sulfate < UroC, in a total amount of 4.73 and 3.81 nmol/g tissue for 50 and 100 mg/kg b.w. CS extract groups, respectively. Sulfated conjugates of EntL were the only lignan metabolites quantified (≈0.90 nmol/g tissue), while catechol and its metabolites corresponded to 14.65 and 13.03 nmol/g tissue, respectively, for 50 and 100 mg/kg b.w. groups. Catechol-*O*-sulfate was the main metabolite, while a substantial fraction (9–15%) of unmetabolized catechol also reached kidney. In summary, sulfated conjugates correspond to 60% of the total metabolites content. Higher concentrations of HPPAs (2442.70 nmol/g tissue), HCAs (80.51 nmol/g tissue), and lignans metabolites (0.94 nmol/g tissue) were achieved for 100 mg/kg b.w. CS extract-treated rats. Considering the 50 mg/kg b.w. CS extract group, higher levels of HBAs (426.80 nmol/g tissue), HPAAs (113.60 nmol/g tissue), pyrogallol (62.48 nmol/g tissue), catechol (14.65 nmol/g tissue) and ellagic acid metabolites (4.73 nmol/g tissue) were determined. Overall, higher concentrations of polyphenols and their metabolites were accumulated in the kidney of

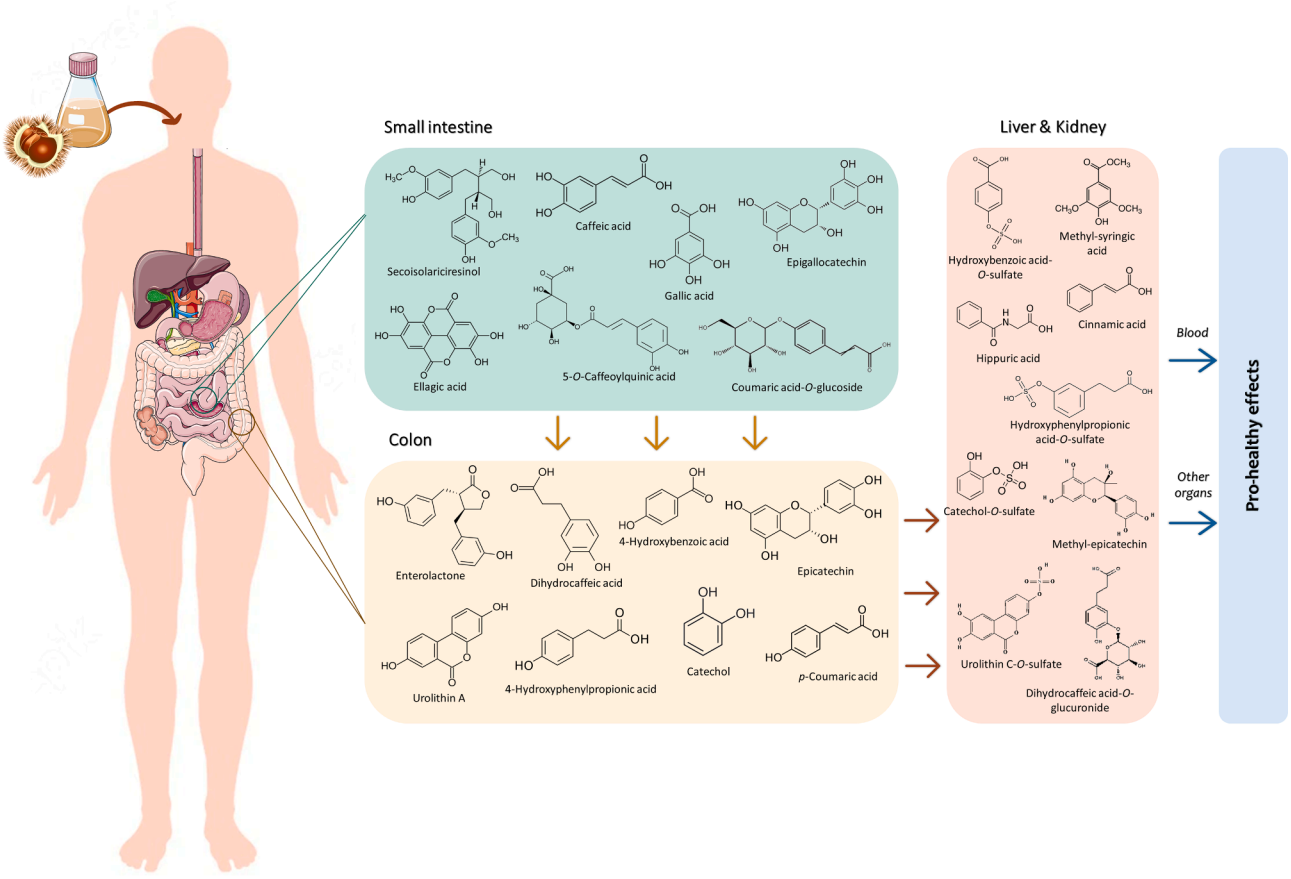

Fig. 2. Schematic representation of the metabolism of chestnut shells extract orally administered to rats.

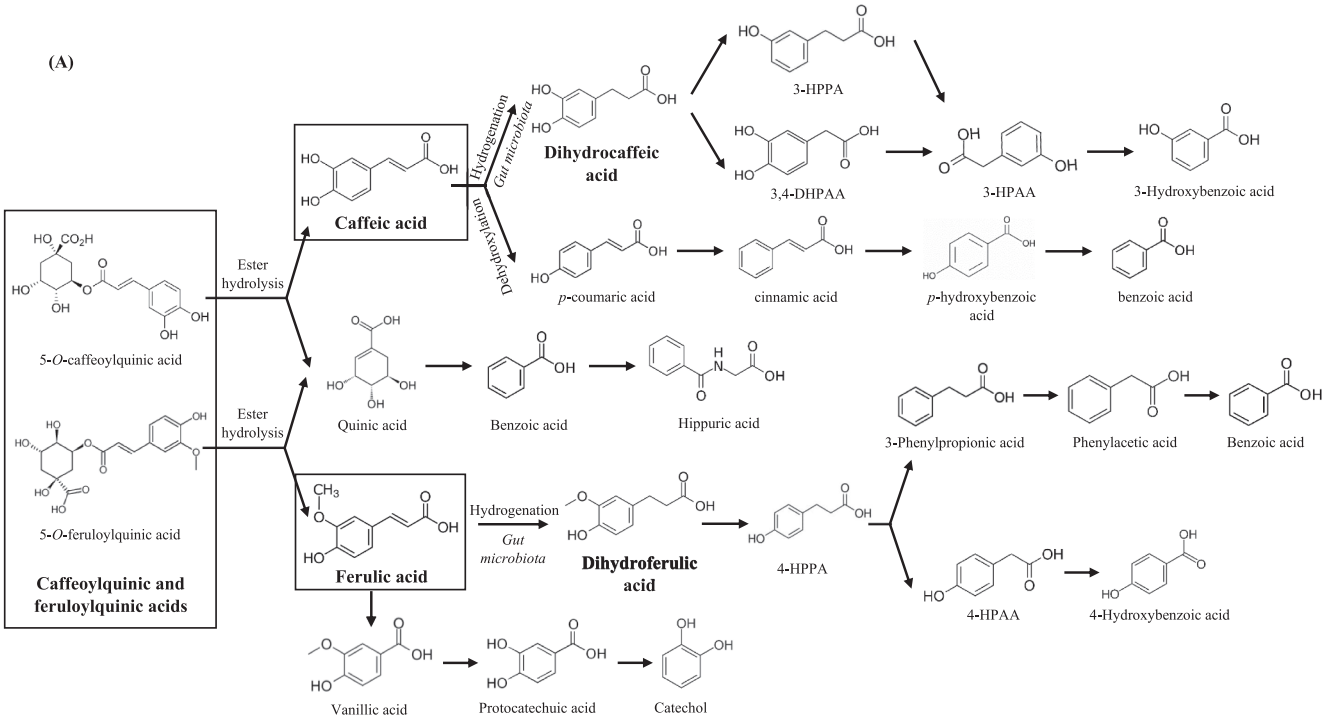

Fig. 3. Metabolic pathways of phenolic compounds. (A) hydroxycinnamic acids; (B) flavanols; (C) gallotannins; (D) ellagic acid; and (E) lignans.

100 mg/kg b.w. group, evidencing an interesting metabolomic profiling that endorses the strong *in-vivo* antioxidant effects proved in our previous study.

There was no direct proportionality between the concentration of phenolic metabolites and the increase of CS extract dose from 50 to 100 mg/kg b.w. The discrepancies on the results between the two extract doses tested may be explained by: i) the saturation of carriers with other molecules, hindering their transport and absorption through intestinal barrier; and ii) the poor reproducibility in the animal research related to high heterogenization of responses and biological variance (López-Yerena, Domínguez-López, et al., 2021; Voelkl et al., 2020).

3.3. Proposed metabolic pathways

3.3.1. Hydroxycinnamic acids

Three possible pathways were proposed for HCAs in this study: i) a minor fraction was absorbed intact in the upper gastrointestinal tract; ii) a small ratio was directly metabolized into glucuronidated, methylated, and sulfated conjugates by phase II enzymes, i.e., uridine diphosphate (UDP)-glucuronosyltransferases, catechol-*O*-methyltransferases and sulfotransferases in liver, kidney and intestine; and iii) a major portion reached the colon, where were metabolized by microbial esterases and reductases or biotransformed into smaller phenolic acids before absorption and conjugation into phase II metabolites (Piazzon et al., 2012; Sova & Saso, 2020). Fig. 2 presents a metabolic scheme of the CS extract. Fig. 3 depicts the metabolic pathways of the polyphenols identified in rat tissues.

Beyond a small fraction that may be absorbed in the upper gastrointestinal tract, caffeoylquinic, feruloylquinic, and coumaroylquinic acids (identified in CS extract) are hydrolyzed in colon via microbial esterases, releasing CA, FA and CoumAc, respectively, which are further conjugated with methyl, sulfate, and glucuronic acid in intestine or liver (Sova & Saso, 2020). This explains the absence of quinic acid derivatives in rat tissues. Additionally, the quinic acid originates benzoic acid (dehydroxylation) that conjugates with acyl glycine producing HippurAc, which was detected in both tissues (Sova & Saso, 2020).

Likewise, phenolic glycosides detected in CS extract, i.e., CA-*O*-glucoside, FA-*O*-glucoside, CoumAc-*O*-glucoside and SinapAc-*O*-glucoside, are partially hydrolyzed in the stomach by glycosidases (regardless the low pH), biotransformed into aglycones in the small intestine (by lactase-phlorizin hydrolase or cytosolic β-glucosidase), converted into phase II metabolites that are transported into liver (where undergo further metabolization) and, finally, enter the bloodstream or return to the digestive tract by enterohepatic circulation (López-Yerena, Domínguez-López, et al., 2021; Sova & Saso, 2020). These mechanisms may also explain the presence of sulfated, methylated, and glucuronidated conjugates of CA, FA, CoumAc, CinnamAc and SinapAc in rat tissues, along with traceable concentrations of their free forms.

Besides, CA may be directly dehydroxylated into *p*-CoumAc and further CinnamAc, whereas FA may be a precursor of vanillic acid, possibly metabolized into protocatechuic acid (via demethylation) and catechol (via decarboxylation) (Sova & Saso, 2020).

Another fraction of HCAs may reach the colon and be metabolized into reduced forms, DHCA and DHFA, by the intestinal microbiota (Alam et al., 2016; Sova & Saso, 2020). These colonic metabolites may be further absorbed through colonic epithelium and then conjugated by phase II enzymes in intestine, liver, and kidney (Sova & Saso, 2020). This metabolic pathway corroborates the high concentrations of DHCA and DHFA and their metabolites detected in rat tissues, along with *p*-CoumAc, CinnamAc and their conjugates. Otherwise, colonic metabolites may undergo enzymatic bioconversion into smaller phenolic acids (Alam et al., 2016; Sova & Saso, 2020). For instance, the dehydroxylation of DHCA generates HPPA, while the loss of carbons originates 3,4-dihydroxyphenylacetic acid.

In summary, HPPAs, HPAAs, and HBAs are among the colonic metabolites of HCAs, followed by their reduced forms (DHCA and DHFA), along with phase II conjugates, which explain their high concentrations in rat tissues, underlying the importance of the gut microbiota in HCAs metabolism. 3-HPPA was indicated as a major metabolite of caffeoylquinic acids in human fecal samples, while DHCA-*O*-sulfate is a potential biomarker of coffee intake, representing 24% of the metabolites excreted (Stalmach et al., 2010). Sulfated conjugates were the major phase II metabolites, followed by methylated and, to a lower extent, glucuronidated conjugates, which agrees with this study findings. These different pathways may extend the permanence of HCAs in the human body contributing to a prolonged *in-vivo* bioactivity, owing to enterohepatic recirculation or colonic absorption. Concerning the bioactivity, previous studies revealed effective scavenging potential against nitric oxide and DPPH radicals for HCAs metabolites (Alam et al., 2016; Piazzon et al., 2012).

3.3.2. Flavanols

Besides acting as radical scavengers, catechins modulate essential signaling pathways, influencing inflammatory, oxidative or cell proliferation processes, and revert metabolic changes induced by high-fat diets (Márquez Campos et al., 2019; Shang et al., 2017). Nonetheless, it is important to comprehend the metabolic pathways of catechins to ascertain their bioactivity (Fig. 3B). Catechin gallates generally maintain stable during gastric passage and are biotransformed by gut microbiota, prior to their detoxification in the liver (Márquez Campos et al., 2019). At intestine, (epi)gallocatechin-*O*-gallate and (epi)catechin-*O*-gallate (present in CS extract) are hydrolyzed by microbial esterases, releasing GA, (epi)gallocatechin and (epi)catechin. Free epi(gallo)catechins are metabolized in the colon through C-ring opening, producing diphenylpropan-2-ol intermediates, further converted into PVL and PVA via A-ring fission. Smaller phenolic acids, including HPPAs and HBAs, are formed by the gut microbiota through successive loss of carbons via β-oxidation (Márquez Campos et al., 2019; Shang et al., 2017). These phenolic acids are easily absorbed and may exert even higher physiological effects than the parent flavonoids (Shang et al., 2017). PVL, PVA and phenolic acids may be bioconverted into phase II metabolites, which are excreted in urine (Márquez Campos et al., 2019; Shang et al., 2017). These metabolic pathways may explain the presence of methylated and sulfated GA, free HPPA and its glucuronidated and sulfated metabolites in liver and kidney. Free catechol and pyrogallol may result from decarboxylation and dehydroxylation of GA, respectively (Shang et al., 2017). HPPA may be metabolized into benzoic acid (dehydroxylation and demethylation) and further conjugated with acyl glycine, originating HippurAc (Shang et al., 2017). This may be also the metabolic source of 4-HBA and its sulfated conjugate.

A small ratio of (epi)catechin was absorbed and directly metabolized by phase II enzymes, explaining the presence of (epi)catechin-*O*-glucuronide and methyl-(epi)catechin in liver (Márquez Campos et al., 2019; Shang et al., 2017). PVL and PVA were not identified in rat tissues, having probably been converted into phenolic acids and their metabolites that were detected in liver and kidney. Beyond the health benefits of HBAs, HippurAc provides antibacterial, anticancer, antifungal, and antiviral properties (Shang et al., 2017).

3.3.3. Hydroxybenzoic acids

HBAs are major metabolites of more complex polyphenols, including HCAs and flavanols (Bento-Silva et al., 2020). Beyond its abundance as free compound, GA may be released from gallotannins and further absorbed, or undergo microbial metabolism via methylation, dehydroxylation and decarboxylation, producing methyl-GA, DHBA and pyrogallol, respectively (Fig. 3C) (Bento-Silva et al., 2020). This metabolic pathway corroborates the presence of GA, methyl gallate and pyrogallol in CS extract, while only two phase I and three phase II metabolites were detected in liver and kidney.

3.3.4. Hydrolysable tannins

Besides its release by hydrolysis of ellagitannins (previously

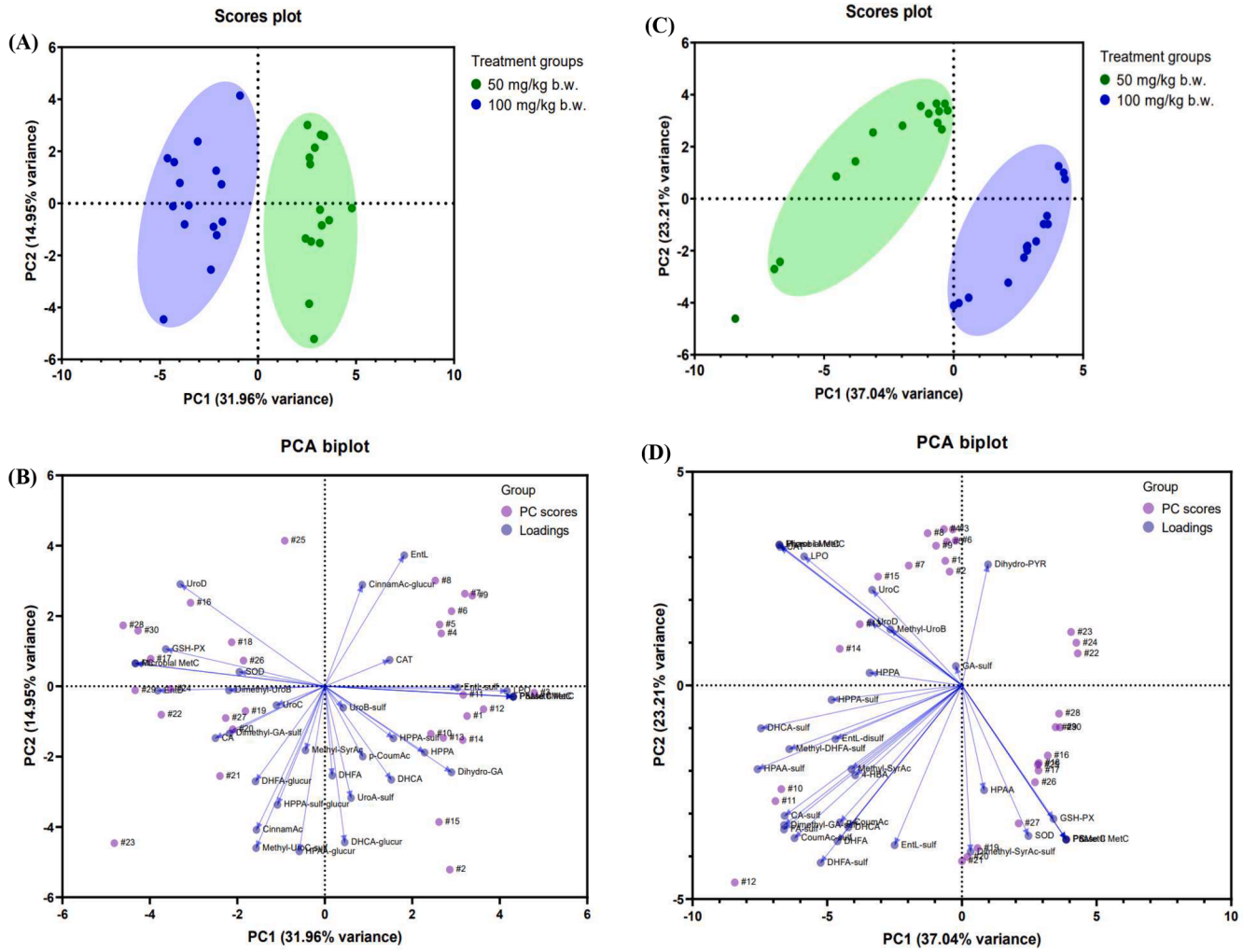

Fig. 4. Principal component analysis on the antioxidant enzymes activities and metabolomic profile of liver and kidney from rats treated with chestnut shells extract at 50 and 100 mg/kg b.w. (A) scores plot from the liver; (B) biplot of variables from the liver; (C) scores plot from the kidney; and (D) biplot of variables from the kidney. CA, caffeic acid. CAT, catalase activity. CinnamAc, cinnamic acid. CL, catechol. DHCA, dihydrocaffeic acid. DHFA, dihydroferulic acid. EntD, enterodiol. EntL, enterolactone. (Epi)CQ, (epi)catechin. FA, ferulic acid. GA, gallic acid. glucur, glucuronide. GSH-Px, glutathione peroxidase activity. HippuricAc, hippuric acid. 4-HBA, 4-hydroxybenzoic acid. HPAA, hydroxyphenylacetic acid. HPPA, hydroxyphenylpropionic acid. LPO, lipid peroxidation. ρ-CoumAc, ρ-Coumaric acid. PYR, pyrogallol. SinapAc, sinapic acid. SOD, superoxide dismutase activity. sulf, sulfate. SyrAc, syringic acid. Uro, urolithin.

identified in CS), ellagic acid may be also present as free compound which could be absorbed at the upper digestive tract and biotransformed by phase II enzymes, explaining the presence of ellagic acid and its dimethylated conjugate in liver (Tomás-Barberán et al., 2014). Otherwise, ellagic acid is converted into urolithins by intestinal microbiota (Tomás-Barberán et al., 2014). UroD is produced through hydrolysis of one lactone and reduction of carboxylic acid into a semi-hydroquinone, followed by dehydroxylation and decarboxylation. Subsequent dehydroxylation produces UroC, UroA and UroB (Fig. 3D) (Tomás-Barberán et al., 2014). Urolithins may be further conjugated with methyl, sulfate, and glucuronic acid, explaining their presence in liver and kidney (Tomás-Barberán et al., 2014). Beyond the pro-healthy properties of ellagic acid, urolithins have attested anti-inflammatory, anticancer, immunomodulatory, neuroprotective, cardioprotective, osteoprotective, and microbiota modulatory effects in animals and humans, highlighting its potential use as effective molecules in the prevention and co-treatment of certain pathological disorders (Laveriano-Santos, Marhuenda-Muñoz, et al., 2022; Laveriano-Santos, Quifer-Rada, et al., 2022).

3.3.5. *Lignans*

Secoisolariciresinol was the only lignan identified in CS extract. Even though trace levels were detected in liver, the highest fraction was metabolized into enterolignans via intestinal microbiota (Fig. 3E). Secoisolariciresinol was metabolized into EntD via *O*-demethylation and dehydroxylation and, then, into EntL by dehydrogenation which were further conjugated with sulfate and glucuronic acid (Li et al., 2022). This metabolic pathway justifies the presence of EntD, EntL and sulfated and glucuronidated metabolites in liver and kidney (Li et al., 2022). An *in-vitro* study using intestinal cells detected EntL-*O*-sulfate, EntL-*O*-glucuronide and EntD-*O*-glucuronide after exposure to lignans (Jansen et al., 2005). EntD and EntL are indicated as the main metabolites responsible for the pro-healthy effects ascribed to lignans, including antioxidant properties and modulation of hormone metabolism, protecting against certain cancers and hair loss (Laveriano-Santos, Marhuenda-Muñoz, et al., 2022; Li et al., 2022).

3.3.6. *Influence of metabolism in the bioavailability and bioactivity of polyphenols*

The relationship between polyphenols and gut microbiota is bidirectional, with microbiota metabolizing polyphenols and, in turn, polyphenols modifying the microbiome by favoring the growth of beneficial bacteria and inhibiting pathogenic species (Corrêa et al., 2019). The microbiota-modulating effect of polyphenols may prevent or

accelerate the recovery of metabolic diseases by strengthening the immune system (Bento-Silva et al., 2020; Corrêa et al., 2019). This is particularly important for HCAs, re-establishing microbiota, reducing pro-inflammatory cytokines secretion and pro-oxidant species, and relieving oxidative stress (Bento-Silva et al., 2020). Additionally, HPAA and HPPA were correlated to *Bifidobacterium* growth with beneficial gut effects (Bento-Silva et al., 2020). Noteworthy, it has been suggested that circulating phenolic metabolites may undergo enzymatic deconjugation at the site of action, despite this mechanism remains still unexplained (Bento-Silva et al., 2020).

Latest advances have attested *in-vivo* bioactivity of plasma and tissues from animals and humans after intake of polyphenols-rich foods, suggesting that phenolic metabolites still retain strong antioxidant properties (Martins et al., 2016; Piazzon et al., 2012). Glucuronidation and sulfation provide more hydrophilic compounds that may affect the bioavailability and site of action (López-Yerena, Domínguez-López, et al., 2021). Piazzon et al. (2012) described identical antioxidant activity for glucuronidated and sulfated metabolites from FA and CA compared to parent compounds. Conjugation reactions may also enhance other biological activities, namely hypolipidemic properties for catechin-methylated conjugates, and antimicrobial properties for glucuronidated and methylated conjugates from 4-HBA, *p*-CoumAc and CinnamAc. Nevertheless, there are few studies about the bioactivity of phenolic metabolites owing to the lack of accurate identification and available of commercial standards (Piazzon et al., 2012).

The production of phenolic acids by colonic metabolism contribute to the bioavailability of polyphenols in a greater extent than phase I and II metabolites. Microbial metabolites represent 45% and 70% of the total content in liver and kidney, respectively, of which 80% correspond to colonic metabolites conjugated with methyl, sulfate, and glucuronic acid.

3.4. Screening of potential oxidative stress biomarkers

PCA has three key assumptions: i) sphericity or existence of the identity matrix; ii) sampling adequacy or an appropriate number of observations relative to the number of variables under analysis; and iii) positive determinant of the correlation or variance–covariance matrices (Bailey, 2012; Spiegelberg & Rusz, 2017). For the first assumption, a Bartlett's test for sphericity was performed to ascertain the veracity of the null hypothesis before proceeding with PCA. The null hypothesis is that the variables are not correlated to each other; if it is true, the PCA is not appropriate since it relies on the construction of a linear combination of the variables (Spiegelberg & Rusz, 2017). The results of Bartlett's test revealed $p < 0.05$, corroborating that at least two of the variables are correlated to each other and, thus, rejecting the null hypothesis (Supplementary Fig. S3). Regarding the second assumption, the sampling adequacy was higher than 0.9 for both liver and kidney tissues which is much higher than the minimum acceptable for PCA application (>0.5) (Spiegelberg & Rusz, 2017). Considering the third assumption, the strong correlations between most variables (demonstrated by the heatmap correlation diagram) underline the rejection of null hypothesis owing to the lack of identity matrix and presence of collinearity among variables creating a correlation matrix (Spiegelberg & Rusz, 2017). Based on the results, the three assumptions were ensured, concluding that it is reasonable to apply a dimension-reduction method to these data capable of reducing data dimensionality and noise. As a valuable statistical tool, PCA (Fig. 4) allows the screening of the phenolic metabolites that contribute to the *in-vivo* antioxidant responses, comprehending the differences among groups regarding metabolomic fingerprinting (evaluated in this study), antioxidant enzymes' activities (SOD, CAT and GSH-Px) and LPO prevention (data previously published (Pinto et al., 2023)).

3.4.1. Liver

The scores plot (Fig. 4A) reveals an evident separation of the treatment groups with 46.91% of explained variance, emphasizing different *in-vivo* antioxidant responses of liver from 50 and 100 mg/kg b.w. CS extract groups. The PC1 explains 31.96% of the results with an eigenvalue of 10.55 (Supplementary Fig. S1). The biplot (Fig. 4B) indicates a strong role of the metabolomic profiling in the *in-vivo* antioxidant properties of liver. A positive correlation is denoted for variables closest and farthest from the diagram origin, while variables situated oppositely are negatively correlated. The plots suggest that the *in-vivo* antioxidant properties of 50 mg/kg b.w. CS extract group (marked green) are strongly ascribed to LPO prevention and contents of EntL, CinnamAc-*O*-glucuronide, EntL-*O*-sulfate, dihydro-GA, HPPA, DHCA, UroA-*O*-sulfate and DHCA-*O*-glucuronide. Considering the highest extract dose tested (marked in blue), GSH-Px activity and contents of UroD, EntD, CA, dimethyl-GA-*O*-sulfate, DHFA-*O*-glucuronide, HPPA-*O*-sulfate-glucuronide, CinnamAc, methyl-UroC-*O*-sulfate, and HPAA-*O*-glucuronide are strongly correlated with its *in-vivo* antioxidant response. Overall, the LPO prevention is the main variable contributing to the *in-vivo* antioxidant activity of liver from 50 mg/kg b.w. group, which is related to phenolic acids and metabolites (mainly HBAs, HCAs and HPPAs), two lignan metabolites and one hydrolysable tannin metabolite. The *in-vivo* antioxidant capacity of liver from 100 mg/kg b.w. group is mainly attributed to GSH-Px activity, corroborated by the microbial metabolites from lignans and hydrolysable tannins, and phenolic acids metabolites from HBAs, HCAs, HPPAs and HPAAs. Additionally, CAT and SOD activities had a small influence on the *in-vivo* bioactivity of liver.

3.4.2. Kidney

The scores plot (Fig. 4C) evidences a clear separation between the two treatment groups. A cumulative variance of 60.24% is pointed out with PC1 explaining 37.04% variance, underlining markedly different *in-vivo* antioxidant responses for 50 and 100 mg/kg b.w. CS extract groups. High eigenvalues were determined for PC1 and PC2 (12.22 and 7.66, respectively), corroborating the explained variance results. The biplot (Fig. 4D) suggests a strong effect of the metabolomic profile on the *in-vivo* antioxidant activity of kidney. The *in-vivo* antioxidant response of kidney from 50 mg/kg b.w. group (marked green) is closely correlated to CAT activity, LPO prevention and contents of UroC, UroD, methyl-UroB, HPPA, HPPA-*O*-sulfate, DHCA-*O*-sulfate, EntL-*O*-disulfate, methyl-DHFA-*O*-sulfate, HPAA-*O*-sulfate, methyl-SyrAc, 4-HBA, CA-*O*-sulfate, FA-*O*-sulfate, dimethyl-GA-*O*-sulfate, *p*-CoumAc, CoumAc-*O*-sulfate, DHCA, DHFA, DHFA-*O*-sulfate, and EntL-*O*-sulfate. Otherwise, the *in-vivo* antioxidant efficacy of 100 mg/kg b.w. group was confirmed by GSH-Px and SOD activities and contents of HPAA and dimethyl-SyrAc-*O*-sulfate. Overall, LPO prevention and CAT activity are the major variables contributing to the *in-vivo* bioactivity of kidneys from 50 mg/kg b.w. group possibly associated to phenolic acids and metabolites (mainly HBAs, HCAs, HPPAs and HPAAs), along with microbial metabolites from lignans and hydrolysable tannins. The *in-vivo* bioactivity of kidneys from 100 mg/kg b.w. group is related to HPAAs and one SyrAc metabolite.

In general, the PCA model pointed out a higher heterogeneity among kidney results when compared to liver. Recently, Pinto et al. (2023) proved marked differences in metabolic profiles and *in-vivo* antioxidant effects of blood serum from rats treated with the same two doses of the CS extract (50 and 100 mg/kg b.w.) analyzed in this study. Phenolic acids, lignans and flavanols, along with their metabolites, were proposed as the major compounds endorsed in the *in-vivo* antioxidant efficacy. Hence, phenolic metabolites and antioxidant enzymes activities may be potential oxidative stress biomarkers whose concentration and activity may vary in response to an increased redox stress. This study proposes that the bioactive molecules from CS extract and their metabolites exert protective effects against oxidative damages, particularly in liver and kidney, induced by pro-oxidant reactive species into biomolecules (i.e., DNA, lipids, and proteins).

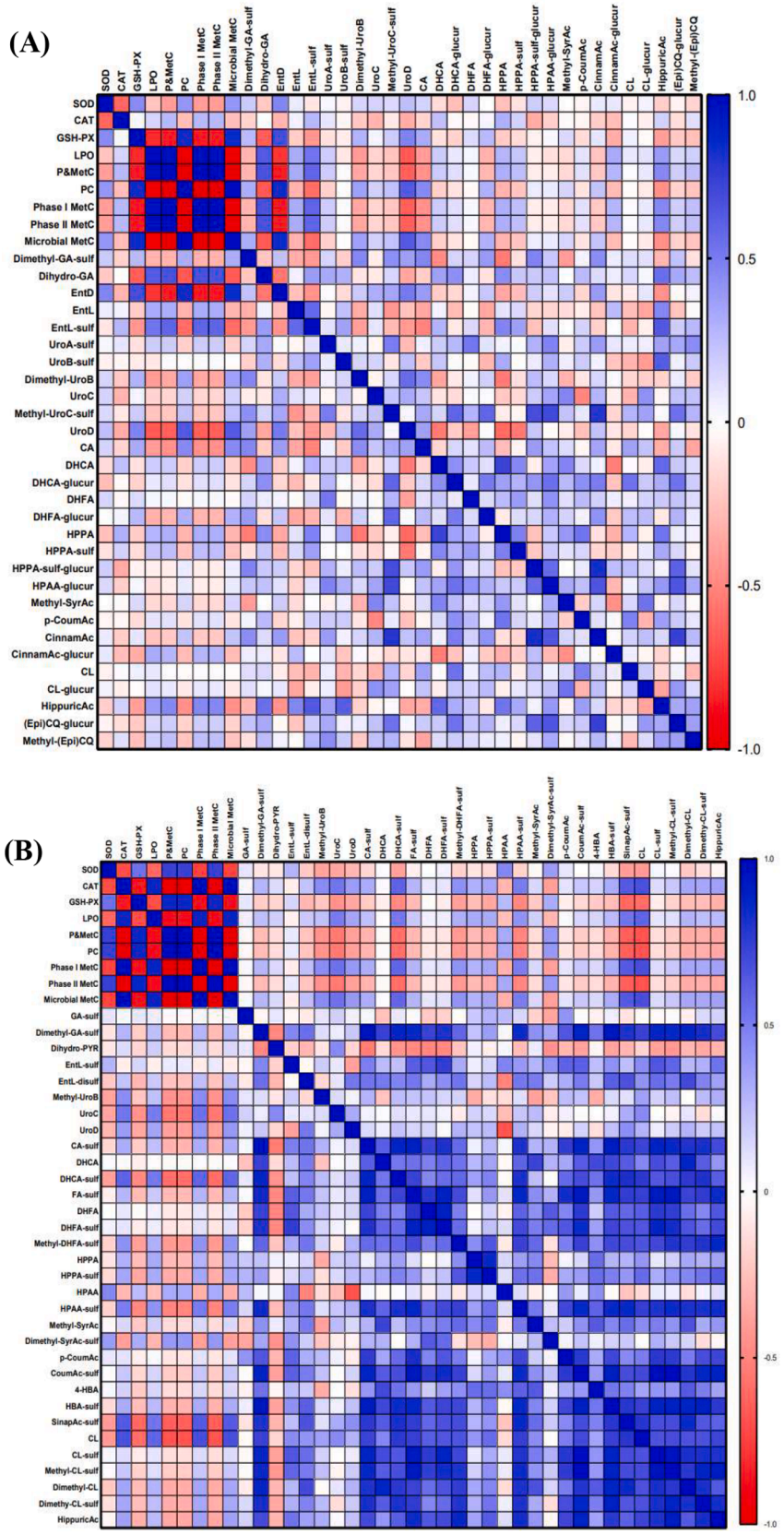

Fig. 5. Correlation heatmap diagram of *in vivo* antioxidant activity and metabolomic profile of (A) liver and (B) kidney from rats treated with chestnut shells extract targeted on phenolic compounds.

3.5. Screening of correlations between metabolic profiling and in-vivo antioxidant response

Several studies have ascribed the *in-vitro* antioxidant activity of plant derivatives to their phenolic composition (Lameirão et al., 2020; Pinto & Cádiz-Gurrea et al., 2020; Pinto, Silva, et al., 2021; Pinto, Vieira, et al., 2021; Rodrigues et al., 2015). However, there is still a lack of studies regarding this correlation on animal experiments. This study provides for the first time a comprehensive assessment of the correlations between *in and vivo* antioxidant activity (evaluated in our previous paper (Pinto et al., 2023)) and metabolomic fingerprinting of tissues from rats orally treated with CS extract through correlation heatmaps (Fig. 5).

Considering the *in-vivo* antioxidant response of liver, a weak positive correlation ($r^2 = 0.447$) was highlighted between SOD and GSH-Px activities. A negative correlation was disclosed between SOD and CAT activities ($r^2 = -0.609$). Likewise, GSH-Px activity was negatively correlated to LPO ($r^2 = -0.812$), denoting that a rise on GSH-Px activity is closely related to a decrease on LPO rate. The SOD and GSH-Px activities of liver were mainly ascribed to the free polyphenols and microbial metabolites identified ($r^2 = 0.402$ and $r^2 = 0.847$, respectively, for SOD and GSH-Px), especially to EntD, UroD and CA ($r^2 > 0.467$). The protective effects against LPO were also attributed to the free polyphenols and microbial metabolites detected in liver owing to a remarkable inverse relation ($r^2 = -0.971$), particularly to EntD, dimethyl-UroB, UroD and CA ($r^2 > -0.510$). Additionally, CAT activity was not correlated to the metabolomic profile.

Regarding the *in-vivo* antioxidant potential of kidney, a strong positive correlation was noticed between CAT activity and LPO prevention ($r^2 = 0.868$), indicating that an increase on CAT activity leads to an exacerbated production of malondialdehyde induced by free radicals. The CAT activity was ascribed in a higher extent to the phase I and microbial metabolites ($r^2 = 0.995$), mainly catechol ($r^2 = 0.671$), SinapAc-*O*-sulfate ($r^2 = 0.631$), DHCA-*O*-sulfate ($r^2 = 0.593$), UroC ($r^2 = 0.523$), HPAA-*O*-sulfate ($r^2 = 0.497$), methyl-UroB ($r^2 = 0.441$), methyl-DHFA-*O*-sulfate ($r^2 = 0.420$), UroD ($r^2 = 0.374$), and HippurAc ($r^2 = 0.359$). Conversely, LPO is negatively correlated with SOD ($r^2 = -0.604$) and GSH-Px ($r^2 = -0.697$), emphasizing an inverse relation in which the increase of SOD and GSH-Px activities leads to a higher LPO prevention. Polyphenols and their metabolites, mainly from phase II reactions ($r^2 = -0.877$), are indicated as the main compounds contributing to the protective effects against LPO. The correlation between SOD and GSH-Px revealed to be positive ($r^2 = 0.538$), with free polyphenols and their phase II metabolites upregulating SOD and GSH-Px activities ($r^2 = 0.736$ and 0.866, respectively, for SOD and GSH-Px) and, accordingly, enhancing the *in-vivo* antioxidant response of kidney. HPAA ($r^2 = 0.458$) and dimethyl-SyrAc-*O*-sulfate ($r^2 = 0.380$) are the major compounds delivering modulatory effects on antioxidant enzymes' activities.

These outcomes emphasize a good correlation level within some variables, outlining an exceptional contribution of the polyphenols and their microbial and phase II metabolites to the *in-vivo* antioxidant responses of liver and kidney through upmodulating antioxidant enzymes' activities and downregulating LPO, which corroborates the PCA results.

Altogether, these correlations seem to be efficient indicators in predicting that phenolic acids and microbial metabolites from lignans and ellagic acid are the major compounds contributing to the *in-vivo* antioxidant response of rats orally treated with CS extract, motivating its use as a nutraceutical ingredient useful in the prevention and co-treatment of lifestyle-related pathologies (i.e., Alzheimer's and Parkinson's diseases, cancer, diabetes, neurological, cardiovascular, and metabolic pathologies) associated to oxidative damages.

4. Conclusion

The current study attempted to pursue the validation of a nutraceutical extract from CS as an appealing source of antioxidants embracing *in-vivo* pro-healthy effects. A metabolomic approach provides novel insights into the bioavailability of polyphenols from CS and the identification of circulating metabolites. Following an in-depth assessment of *in-vitro* and *in-vivo* biological effects accomplished in recent studies, the metabolomic profile of different tissues from rats orally treated with phenolics-rich CS extract corroborated the promising outcomes regarding its *in-vivo* bioactivity. Unmetabolized polyphenols, along with their phase I and II metabolites, were noticed in both tissues with higher accumulation in kidney. Phenolic acids were the major polyphenolic class in rat tissues, followed by hydrolysable tannins, flavanols and lignans. Sulfated conjugates were the main metabolites reaching kidney, while liver contained identical concentrations of glucuronidated, methylated, and sulfated metabolites. The multivariate data analysis predicted an outstanding contribution of polyphenols and their microbial and phase II metabolites to the *in-vivo* antioxidant efficacy of CS extract in rats, proposing its use as a prominent source of anti-aging molecules for nutraceuticals with health benefits in the prevention and co-therapy of lifestyle-related diseases triggered by oxidative stress. Further studies will be focused on designing a nutraceutical product incorporating CS extract and evaluate its efficacy and safety.

CRediT authorship contribution statement

Diana Pinto: Methodology, Software, Formal analysis, Investigation, Writing – original draft. **Anallely López-Yerena:** Methodology, Formal analysis, Investigation, Writing – review & editing. **Andreia Almeida:** Methodology, Formal analysis, Investigation, Writing – review & editing. **Bruno Sarmento:** Methodology, Funding acquisition, Resources. **Rosa Lamuela-Raventós:** Methodology, Funding acquisition, Resources. **Anna Vallverdú-Queralt:** Methodology, Supervision, Writing – review & editing. **Cristina Delerue-Matos:** Methodology, Supervision, Resources. **Francisca Rodrigues:** Methodology, Conceptualization, Validation, Investigation, Resources, Writing – review & editing, Supervision, Project administration, Funding acquisition.

Declaration of Competing Interest

The authors declare that they have no known competing financial interests or personal relationships that could have appeared to influence the work reported in this paper.

Data availability

The authors do not have permission to share data.

Acknowledgments

The authors kindly thanks Sortegel (Sortes, Portugal) for the samples. This work received financial support from national funds (UIDB/50006/2020), project PTDC/ASP-AGR/29277/2017 - *Castanea sativa* shells as a new source of active ingredients for Functional Food and Cosmetic applications: a sustainable approach, and project 5537 DRI, Sérvia 2020/21 from Portuguese-Serbia Bilateral Cooperation - Development of functional foods incorporating a chestnut shells extract obtained by subcritical water, supported by national funds by FCT/MCTES and co-supported by Fundo Europeu de Desenvolvimento Regional (FEDER) throughout COMPETE 2020 - Programa Operacional Competitividade e Internacionalização (POCI-01-0145-FEDER-029277). Diana Pinto is thankful for her Ph.D. grant (SFRH/BD/144534/2019) financed by FCT/MCTES and POPH-QREN and supported by funds from European Union (EU) and Fundo Social Europeu (FSE) through Programa Operacional Regional Norte. Francisca Rodrigues is grateful for her contract (CEECIND/01886/2020) financed by FCT/MCTES—CEEC Individual 2020 Program Contract. Anna Vallverdú-Queralt thanks the Spanish Ministerio de Ciencia, Innovación y Universidades for the Ramon y Cajal contract (RYC-2016-19355).

Appendix A. Supplementary material

Supplementary data to this article can be found online at https://doi.org/10.1016/j.foodres.2023.112963.

References

Alam, M. A., Subhan, N., Hossain, H., Hossain, M., Reza, H. M., Rahman, M. M., & Ullah, M. O. (2016). Hydroxycinnamic acid derivatives: A potential class of natural compounds for the management of lipid metabolism and obesity. *Nutrition & Metabolism, 13*, 27. https://doi.org/10.1186/s12986-016-0080-3

Bailey, S. (2012). Principal component analysis with noisy and/or missing data. *Publications of the Astronomical Society of the Pacific, 124*, 1015–1023. https://doi.org/10.1086/668105

Bento-Silva, A., Koistinen, V. M., Mena, P., Bronze, M. R., Hanhineva, K., Sahlstrøm, S., … Aura, A. M. (2020). Factors affecting intake, metabolism and health benefits of phenolic acids: Do we understand individual variability? *European Journal of Nutrition, 59*, 1275–1293. https://doi.org/10.1007/s00394-019-01987-6

Bhat, F. M., Sommano, S. R., Riar, C. S., Seesuriyachan, P., Chaiyaso, T., & Prom-u-Thai, C. (2020). Status of bioactive compounds from bran of pigmented traditional rice varieties and their scope in production of medicinal food with nutraceutical importance. *Agronomy, 10*, 1817. https://www.mdpi.com/2073-4395/10/11/1817.

Charles, D., Gethings, L. A., Potts, J. F., Burney, P. G. J., & Garcia-Larsen, V. (2021). Mass spectrometry-based metabolomics for the discovery of candidate markers of flavonoid and polyphenolic intake in adults. *Scientific Reports, 11*, 5801. https://doi.org/10.1038/s41598-021-85190-w

Corrêa, T. A. F., Rogero, M. M., Hassimotto, N. M. A., & Lajolo, F. M. (2019). The two-way polyphenols-microbiota interactions and their effects on obesity and related metabolic diseases. *Frontiers in Nutrition, 6*, 188. https://doi.org/10.3389/fnut.2019.00188

Escobar-Avello, D., Mardones, C., Saéz, V., Riquelme, S., von Baer, D., Lamuela-Raventós, R. M., & Vallverdú-Queralt, A. (2021). Pilot-plant scale extraction of phenolic compounds from grape canes: Comprehensive characterization by LC-ESI-LTQ-Orbitrap-MS. *Food Research International, 143*, Article 110265. https://doi.org/10.1016/j.foodres.2021.110265

Jansen, G. H., Arts, I. C., Nielen, M. W., Müller, M., Hollman, P. C., & Keijer, J. (2005). Uptake and metabolism of enterolactone and enterodiol by human colon epithelial cells. *Archives of Biochemistry and Biophysics, 435*, 74–82. https://doi.org/10.1016/j.abb.2004.12.015

Lameirão, F., Pinto, D., Vieira, E. F., Peixoto, A., Freire, C., Sut, S., … Rodrigues, F. (2020). Green-sustainable recovery of phenolic and antioxidant compounds from industrial chestnut shells using ultrasound-assisted extraction: Optimization and evaluation of biological activities *in vitro*. *Antioxidants, 9*, 267. https://www.mdpi.com/2076-3921/9/3/267.

Laveriano-Santos, E. P., Marhuenda-Muñoz, M., Vallverdú-Queralt, A., Martínez-Huélamo, M., Tresserra-Rimbau, A., Miliarakis, E., … Lamuela-Raventós, R. M. (2022). Identification and quantification of urinary microbial phenolic metabolites by HPLC-ESI-LTQ-Orbitrap-HRMS and their relationship with dietary polyphenols in adolescents. *Antioxidants, 11*, 1167. https://www.mdpi.com/2076-3921/11/6/1167.

Laveriano-Santos, E. P., Quifer-Rada, P., Marhuenda-Muñoz, M., Arancibia-Riveros, C., Vallverdú-Queralt, A., Tresserra-Rimbau, A., … Lamuela-Raventós, R. M. (2022). Microbial phenolic metabolites in urine are inversely linked to certain features of metabolic syndrome in Spanish adolescents. *Antioxidants, 11*, 2191. https://www.mdpi.com/2076-3921/11/11/2191.

Li, Y.-X., Pan, Y. G., He, F. P., Yuan, M. Q., & Li, S. B. (2016). Pathway analysis and metabolites identification by metabolomics of etiolation substrate from fresh-cut Chinese water chestnut (*Eleocharis tuberosa*). *Molecules, 21*, 1648. https://doi.org/10.3390/molecules21121648

Li, Y., Wang, F., Li, J., Ivey, K. L., Wilkinson, J. E., Wang, D. D., … Rimm, E. B. (2022). Dietary lignans, plasma enterolactone levels, and metabolic risk in men: Exploring the role of the gut microbiome. *BMC Microbiology, 22*, 82. https://doi.org/10.1186/s12866-022-02495-0

Llorach, R., Garrido, I., Monagas, M., Urpi-Sarda, M., Tulipani, S., Bartolome, B., & Andres-Lacueva, C. (2010). Metabolomics study of human urinary metabolome modifications after intake of almond (*Prunus dulcis* (Mill.) D.A. Webb) skin polyphenols. *Journal of Proteome Research, 9*, 5859–5867. https://doi.org/10.1021/pr100639v

López-Yerena, A., Domínguez-López, I., Vallverdú-Queralt, A., Pérez, M., Jáuregui, O., Escribano-Ferrer, E., & Lamuela-Raventós, R. M. (2021). Metabolomics technologies for the identification and quantification of dietary phenolic compound metabolites: An overview. *Antioxidants, 10*, 846. https://doi.org/10.3390/antiox10060846

López-Yerena, A., Vallverdú-Queralt, A., Jáuregui, O., Garcia-Sala, X., Lamuela-Raventós, R. M., & Escribano-Ferrer, E. (2021). Tissue distribution of oleocanthal and its metabolites after oral ingestion in rats. *Antioxidants, 10*, 688. https://www.mdpi.com/2076-3921/10/5/688.

Luzardo-Ocampo, I., Campos-Vega, R., Gaytán-Martínez, M., Preciado-Ortiz, R., Mendoza, S., & Loarca-Piña, G. (2017). Bioaccessibility and antioxidant activity of free phenolic compounds and oligosaccharides from corn (*Zea mays* L.) and common bean (*Phaseolus vulgaris* L.) chips during *in vitro* gastrointestinal digestion and simulated colonic fermentation. *Food Research International, 100*, 304–311. https://doi.org/10.1016/j.foodres.2017.07.018

Marhuenda-Muñoz, M., Laveriano-Santos, E. P., Tresserra-Rimbau, A., Lamuela-Raventós, R. M., Martínez-Huélamo, M., & Vallverdú-Queralt, A. (2019). Microbial phenolic metabolites: Which molecules actually have an effect on human health? *Nutrients, 11*, 2725. https://www.mdpi.com/2072-6643/11/11/2725.

Márquez Campos, E., Stehle, P., & Simon, M.-C. (2019). Microbial metabolites of flavan-3-ols and their biological activity. *Nutrients, 11*, 2260. https://www.mdpi.com/2072-6643/11/10/2260.

Martins, N., Barros, L., & Ferreira, I. C. F. R. (2016). *In vivo* antioxidant activity of phenolic compounds: Facts and gaps. *Trends in Food Science & Technology, 48*, 1–12. https://doi.org/10.1016/j.tifs.2015.11.008

Noh, J.-R., Gang, G.-T., Kim, Y.-H., Yang, K.-J., Hwang, J.-H., Lee, H.-S., … Lee, C.-H. (2010). Antioxidant effects of the chestnut (*Castanea crenata*) inner shell extract in t-BHP-treated HepG2 cells, and CCl_4- and high-fat diet-treated mice. *Food and Chemical Toxicology, 48*, 3177–3183. https://doi.org/10.1016/j.fct.2010.08.018

Noh, J. R., Kim, Y. H., Gang, G. T., Hwang, J. H., Lee, H. S., Ly, S. Y., … Lee, C. H. (2011). Hepatoprotective effects of chestnut (*Castanea crenata*) inner shell extract against chronic ethanol-induced oxidative stress in C57BL/6 mice. *Food and Chemical Toxicology, 49*, 1537–1543. https://doi.org/10.1016/j.fct.2011.03.045

Piazzon, A., Vrhovsek, U., Masuero, D., Mattivi, F., Mandoj, F., & Nardini, M. (2012). Antioxidant activity of phenolic acids and their metabolites: Synthesis and antioxidant properties of the sulfate derivatives of ferulic and caffeic acids and of the acyl glucuronide of ferulic acid. *Journal of Agricultural and Food Chemistry, 60*, 12312–12323. https://doi.org/10.1021/jf304076z

Pinto, D., Almeida, A., López-Yerena, A., Pinto, S., Sarmento, B., Lamuela-Raventós, R., … Rodrigues, F. (2023). Appraisal of a new potential antioxidants-rich nutraceutical ingredient from chestnut shells through *in-vivo* assays – A targeted metabolomic approach in phenolic compounds. *Food Chemistry, 404*, Article 134546. https://doi.org/10.1016/j.foodchem.2022.134546

Pinto, D., Cádiz-Gurrea, M.d.l. L., Garcia, J., Saavedra, M. J., Freitas, V., Costa, P., … Rodrigues, F. (2021). From soil to cosmetic industry: Validation of a new cosmetic ingredient extracted from chestnut shells. *Sustainable Materials and Technologies, 29*, e00309.

Pinto, D., Cádiz-Gurrea, M.d.l. L., Sut, S., Ferreira, A. S., Leyva-Jimenez, F. J., Dall'Acqua, S., … Rodrigues, F. (2020). Valorisation of underexploited *Castanea sativa* shells bioactive compounds recovered by supercritical fluid extraction with CO_2: a response surface methodology approach. *Journal of CO2 Utilization, 40*, Article 101194. https://doi.org/10.1016/j.jcou.2020.101194

Pinto, D., Cádiz-Gurrea, M. d. l. L., Vallverdú-Queralt, A., Delerue-Matos, C., & Rodrigues, F. (2021). *Castanea sativa* shells: A review on phytochemical composition, bioactivity and waste management approaches for industrial valorization. *Food Research International, 144*, 110364. doi: 10.1016/j.foodres.2021.110364.

Pinto, D., Silva, A. M., Freitas, V., Vallverdú-Queralt, A., Delerue-Matos, C., & Rodrigues, F. (2021). Microwave-assisted extraction as a green technology approach to recover polyphenols from *Castanea sativa* shells. *ACS Food Science & Technology, 1*, 229–241. https://doi.org/10.1021/acsfoodscitech.0c00055

Pinto, D., Vieira, E. F., Peixoto, A. F., Freire, C., Freitas, V., Costa, P., … Rodrigues, F. (2021). Optimizing the extraction of phenolic antioxidants from chestnut shells by subcritical water extraction using response surface methodology. *Food Chemistry, 334*, Article 127521. https://doi.org/10.1016/j.foodchem.2020.127521

Rodrigues, F., Santos, J., Pimentel, F. B., Braga, N., Palmeira-de-Oliveira, A., & Oliveira, M. B. (2015). Promising new applications of *Castanea sativa* shell: Nutritional composition, antioxidant activity, amino acids and vitamin E profile. *Food and Function, 6*, 2854–2860. https://doi.org/10.1039/c5fo00571j

Rudrapal, M., Khairnar, S. J., Khan, J., Dukhyil, A. B., Ansari, M. A., Alomary, M. N., … Devi, R. (2022). Dietary polyphenols and their role in oxidative stress-induced human diseases: Insights into protective effects, antioxidant potentials and mechanism(s) of action. *Frontiers in Pharmacology, 13*, Article 806470. https://doi.org/10.3389/fphar.2022.806470

Sasot, G., Martínez-Huélamo, M., Vallverdú-Queralt, A., Mercader-Martí, M., Estruch, R., & Lamuela-Raventós, R. M. (2017). Identification of phenolic metabolites in human urine after the intake of a functional food made from grape extract by a high resolution LTQ-Orbitrap-MS approach. *Food Research International, 100*, 435–444. https://doi.org/10.1016/j.foodres.2017.01.020

Shang, Z., Wang, F., Dai, S., Lu, J., Wu, X., & Zhang, J. (2017). Profiling and identification of (−)-epicatechin metabolites in rats using ultra-high performance liquid chromatography coupled with linear trap-Orbitrap mass spectrometer. *Drug Testing and Analysis, 9*, 1224–1235. https://doi.org/10.1002/dta.2155

Sova, M., & Saso, L. (2020). Natural sources, pharmacokinetics, biological activities and health benefits of hydroxycinnamic acids and their metabolites. *Nutrients, 12*, 2190. https://www.mdpi.com/2072-6643/12/8/2190.

Spiegelberg, J., & Rusz, J. (2017). Can we use PCA to detect small signals in noisy data? *Ultramicroscopy, 172*, 40–46. https://doi.org/10.1016/j.ultramic.2016.10.008

Stalmach, A., Steiling, H., Williamson, G., & Crozier, A. (2010). Bioavailability of chlorogenic acids following acute ingestion of coffee by humans with an ileostomy. *Archives of Biochemistry and Biophysics, 501*, 98–105. https://doi.org/10.1016/j.abb.2010.03.005

Tomás-Barberán, F. A., García-Villalba, R., González-Sarrías, A., Selma, M. V., & Espín, J. C. (2014). Ellagic acid metabolism by human gut microbiota: Consistent observation of three urolithin phenotypes in intervention trials, independent of food source, age, and health status. *Journal of Agricultural and Food Chemistry, 62*, 6535–6538. https://doi.org/10.1021/jf5024615

Tu, J., Li, Q., & Zhou, B. (2021). The tannins from *Sanguisorba officinalis* L. (Rosaceae): A systematic study on the metabolites of rats based on HPLC-LTQ-Orbitrap MS(2) analysis. *Molecules, 26*, 4053. https://doi.org/10.3390/molecules26134053

Voelkl, B., Altman, N. S., Forsman, A., Forstmeier, W., Gurevitch, J., Jaric, I., … Würbel, H. (2020). Reproducibility of animal research in light of biological variation. *Nature Reviews Neuroscience, 21*, 384–393. https://doi.org/10.1038/s41583-020-0313-3